Preprints.org

Article

3,5-dimethyl-2,4,6-trimethoxychalcone Lessens Obesity and Metabolic Dysfunction-Associated Fatty *Liver* Disease (MAFLD) in Leptin-Deficient ob/ob Mice

Stéphanie Gaige , Anne Abysique , Rym Barbouche , Attilio Di Maio , Maxime Robin , Anh Tuan Lormier [*] , Jean-Denis Troadec [*]

Article

3,5-dimethyl-2,4,6-trimethoxychalcone Lessens Obesity and Metabolic Dysfunction-Associated Fatty *Liver* Disease (MAFLD) in Leptin-Deficient ob/ob Mice

Stéphanie Gaige [1,†], Anne Abysique [1,†], Rym Barbouche [1], Attilio Di Maio [3], Maxime Robin [2,3], Anh Tuan Lormier [3,*] and Jean-Denis Troadec [1,*]

[1]   Aix-Marseille University, Centre de Recherche en Psychologie et Neurosciences (CRPN), CNRS UMR 7077, 13331 Marseille, France ; stephanie.gaige@univ-amu.fr; anne.abysique@univ-amu.fr; rym.barbouche@univ-amu.fr

[2]   Aix-Marseille University, Avignon University CNRS, IRD, IMBE, 13013 Marseille, France ; attilio.dimaio@imbe.fr; maxime.robin@univ-amu.fr

[3]   CAYLAB, Contract Research Organization, Istres, France. Anh-Tuan@caylab.fr

*   Correspondence: anh-tuan@caylab.fr (A.T.L.); j-d.troadec@univ-amu.fr (J.-D.T.)

[†]   These authors contributed equally to the present work.

Abstract: Chalcones constitute an important group of natural compounds abundant in fruits and comestible plants. They are a subject of increasing interest because of their biological activities including antidiabetic and anti-obesity effects. The simple chalcone structural scaffold can be modified at multiple sites with different chemical moieties. Here we generated an artificial chalcone, i.e., 3,5-dimethyl-2,4,6-trimethoxychalcone (TriMetChalc), derived from 2′,4′-Dihydroxy-6′-methoxy-3′,5′-dimethylchalcone (DMC). DMC is the major compound of *Cleistocalyx operculatus*, a plant widely used in Asia for its anti-hyperglycemic activity. Using *ob/ob* mice as an obesity model, we ported that, after 3 weeks of *per os* administration, TriMetChalc modified food intake through the specific activation of brain structures dedicated to the regulation of energy balance. TriMetChalc also decreased weight gain, glucose intolerance and hepatic steatosis. Moreover, through extensive liver lipidomic analysis, we identified TriMetChalc-induced modifications that could contribute to improving the liver status of the animals. Hence, TriMetChalc is a chalcone derivative capable of reducing food intake and addition of glucose intolerance, and hepatic steatosis in a mouse model of obesity. In light of these results, we believe that TriMetChalc action deserves to be more deeply evaluated over longer treatment periods and/or in combination with other chalcones with protective effects on the liver.

Keywords: chalcone; food intake; brainstem; hypothalamus; leptin; steatosis; liver

1. Introduction

Keeping a healthy weight has become both a personal challenge and a major public health issue. The majority of people on the planet actually reside in countries where being overweight or obese is associated with a higher death rate than being underweight. The rate of obesity worldwide has almost tripled since 1975. In 2016, there were approximately 1.9 billion obese adults (those above the age of 18). Of these, more than 650 million were overweight. The World Health Organization has estimated that 39 million children under the age of five and over 340 million children and adolescents will be overweight or obese after 2020 [1]. Fat accumulation in the liver, a defining feature of fatty liver disease, is frequently linked to metabolic syndromes, including obesity. Non-alcoholic fatty liver disease (NAFLD) is a term used to cover a continuum of liver disorders that are characterized by evidence of excessive fat in the liver (hepatic steatosis) and the absence of secondary origins (alcohol

consumption, medications, and hereditary disorders). NAFLD is the most common cause of chronic liver disease worldwide and represents a major, expanding public health problem [2]. Over one billion people worldwide suffer from NAFLD, which has become the most common form of chronic liver disease. While the majority of people with fatty liver have no or few symptoms, a small subset can develop liver cancer, or end-stage liver disease [3]. To better reflect the metabolic related etiology of this pathology, a new nomenclature was proposed [4,5]. The term metabolic dysfunction-associated fatty liver disease (MAFLD) is now largely accepted and used. The global epidemic of fatty liver disease grows alongside the obesity pandemic. The prevalence rate of MAFLD rises with increasing body mass index (BMI). Based on data from 1989 to 2015, the global prevalence of MAFLD in the general population has been estimated to be 25% [6]. The prevalence of MAFLD was 17% in lean individuals and between 50% and 90% in the obese population [7]. For instance, based on histologic analysis of liver originating from donor automobile crash victims, autopsy findings, and clinical liver biopsies, the observed prevalence rates of steatosis are approximately 15% in non-obese persons, 65% in persons with class I and II obesity (BMI 30.0–39.9 kg/m^2), and 85% in extremely obese patients (BMI ≥40 kg/m^2) [8].

The need for new compounds and possible treatments to prevent the development of obesity and MAFLD persists, despite the wealth of information on the etiology and mechanisms underlying these pathologies. A class of natural flavonoids derivatives of aromatic ketones known as 1,3-diphenyl-2-propen-1-ones, or chalcones, has attracted attention among natural promising chemicals. This interest is based on their numerous biological actions, including anti-obesity and antidiabetic qualities in both in vitro and in vivo systems. Many plant-derived forms of chalcone with multiple substitution patterns on both aromatic rings, such as hydroxy, methyl, and methoxy substituents, have been identified [9].

2′,4′-Dihydroxy-6′-methoxy-3′,5′-dimethylchalcone (DMC) is the major compound of *Cleistocalyx operculatus*, a plant that is widely distributed in southern Asia. Locally, the water extract of *Cleistocalyx operculatus* is commonly used for its anti-hyperglycemic activity [10]. It was reported that DMC promoted glucose uptake and lipid storage in differentiated 3T3-L1 adipocytes [11] and increased glucose uptake and fatty acid oxidation in myotubes [12]. In addition, DMC improved glucose tolerance and significantly increased fatty acid activation (FAO) of the muscles of high-fat diet (HFD)-fed mice [12]. Chalcones can not only be biosynthesized by plants but can also be manufactured synthetically. The simple chalcone structural scaffold can be modified at multiple sites with different chemical moieties. The resulting molecules could respond to different molecular targets or interfere with different signaling pathways [13–15]. Using a simple synthetic method, we have generated a new artificial chalcone i.e., 3,5-dimethyl-2,4,6-trimethoxychalcone (TriMetChalc) which derived from the 2′,4′-Dihydroxy-6′-methoxy-3′,5′-dimethylchalcone (DMC). Therefore, the aim of this study was to test the effect of TriMetChalc on food intake and weight gain in lean C57Bl/6J mice and leptin-deficient *ob/ob* mice and to evaluate the impact of this molecule on hepatic steatosis that occurs naturally in *ob/ob* mice.

2. Results

2.1. Effect of Acute per os Administration of TriMetChal on Food Intake in C57Bl/6 Mice

A single oral administration of TriMetChal resulted in a dose-dependent decrease in daily food intake in C57Bl/6 mice (Figure 2A). Note that 6.5 and 65 mg/kg BW failed to modify food intake measured during the first 24 hours (h) following administration while 130 and 650 mg/kg BW of TriMetChal diminished it respectively by 11.8 and 18.4%. Food consumption measured 3, 12 and 24 h after treatment revealed that 130 and 650 mg/kg BW TriMetChal mainly affected the night-time food intake (Figure 2B). To decipher feeding behavior analysis after TriMetChalc administration, we quantified the consumption of a non-nutritive substance i.e., kaolin. This behavior, known as pica, serves as a model for the study of nausea/emesis in rodents [20]. Lithium chloride (150 mg/kg BW) well known to induce discomfort in rodents served as positive control. Mice treated with vehicle consumed 0.14 +/- 0.03 mg/24h of kaolin and those treated with lithium ingested 0.33 +/- 0.08 mg/24h

(Figure 2C). While the higher dose of TriMetChalc 650 mg/kg BW caused a significant increase in kaolin intake (0.27 +/- 0.03 mg/24h; P<0.01), at the dose of 130 mg/kg BW TriMetChalc did not induce significant kaolin intake (0.19 +/- 0.02 mg/24h).

2.2. Brain Pattern of Central Pathways Activated in Response t Acute Trimetchalc per os Administration

Central structures activated in response to *per os* administration of 130 mg/kg BW TriMetChalc were next identified using the immune detection of the early gene c-Fos. A very low basal level of c-Fos positive nuclei was observed in the brainstem, pons and forebrain of vehicle-treated mice. TriMetChalc-treated mice showed a strong increase in the number of c-Fos positive nuclei within the nucleus tractus solitarius (NTS) regardless the rostro-caudal level considered and a moderate increase within the area postrema (AP, Figure 3A,B). Animals challenged with TriMetChalc also displayed a strong rise in c-Fos immunoreactivity in the within forebrain structures such as the arcuate nucleus (ARC), paraventricular hypothalamus nucleus (PVN) and ventromedial hypothalamus (VMH; Figure 3C,D).

2.3. Effect of Acute per os Administration of TriMetChalc on Food Intake and c-Fos Expression in ob/ob Mice

The *ob* mutation is a spontaneous recessive mutation in the gene encoding leptin. Mice homozygous for this mutation are leptin deficient and develop obesity which appears around 4-5 weeks of age. In this model, obesity is associated with hyperphagia, hyperglycemia and type II diabetes. To shed light on the mechanisms by which TriMetChalc reduces food intake, we tested the potential interaction between TriMetChalc and endogenous leptin. Thus, we next tested the acute administration of TriMetChalc in *ob/ob* mice. As previously observed in C57Bl/6 mice, TriMetChalc 130 and 650 mg/kg BW reduced night-time food intake (Figure 4A,B). The extend of TriMetChalc-induced food reduction in C57Bl/6 and *ob/ob* mice were similar (Figures 2 and 4). As previously observed with C57Bl/6 mice, TriMetChalc increased kaolin intake at the dose of 650 mg/kg BW but not when administered at 130 mg/kg BW (Figure 4C). c-Fos immunochemistry performed in *ob/ob* mice confirmed this observation. The brain pattern and number of c-Fos positive cells in response to TriMetChalc in *ob/ob* mice resembled those observed in C57Bl/6. Indeed, an increase in c-Fos positive cells was observed in the NTS, the AP and several nuclei of the hypothalamus i.e., PVN, ARC and VMH (Figure 5A–D). Other regions appeared virtually devoid of c-Fos positive nuclei (Figure 5A,B).

2.4. Effect of Chronic TriMetChalc Treatment on Food Intake and Body Weight of Leptin Deficient Mice

We next sought to determine whether the anorexigenic effect of TriMetChalc could reverse leptin deficiency induced-obesity. To this aim, *ob/ob* mice were chronically administered with TriMetChalc once a day during three weeks. We chose to use TriMetChalc at a dose of 65 mg/kg BW, which appeared as a subthreshold dose in experiments measuring 24h food intake over its acute administration. Chronic TriMetChalc administration limited the weight gain of *ob/ob* mice over the period studied (Figure 6A,B). Weight gain was 7.1 +/- 1.4 g for mice that received vehicle and 4.0 +/- 1.6 g for those treated with TriMetChalc (Figure 6A,B). At the same time, cumulative food intake over 3 weeks was reduced by 20.9 +/- 5.6 % by TriMetChalc administration (Figure 6C,D). Interestingly, daily food intake was not significantly reduced in the first week but was decreased from day 7 until the end of treatment (Figure 6D) suggesting a cumulative effect of TriMetChalc. We next evaluated the potential impact of chronic TriMetChalc treatment on glucose intolerance since *ob/ob* mice develop hyperglycemia and a type II diabetes syndrome. OGTT was performed before and after three weeks treatment with 65 mg/kg BW TriMetChalc. The results confirmed the development of glucose intolerance over time in this model (Figure 6E,F). TriMetChalc significantly reduced glycemic response to oral glucose overload in *ob/ob* mice with a more rapid return to basal glycaemia in treated group than control animals (Figure 6E). Quantification of the area under the curve confirmed this observation (Figure 6F).

2.5. Effect of Chronic TriMetChalc Treatment on Hepatic Lipid Content of ob/ob Mice

After the animal sacrifice, observation of livers from TriMetChalc-treated mice (65 mg/kg BW) revealed a slightly less yellow coloration suggesting reduced lipids storage in the test group (data not shown). Weighing the livers after three weeks of treatment showed that TriMetChalc significantly reduced the weight of this organ (Figure 7A). ORO staining is a commonly used experimental technique to detect lipid content in cells or tissues. As shown in Figure 7B, ORO staining confirmed lipid liver storage in *ob/ob* mice and a reduced accumulation in TriMetChalc-treated animals. Quantification of ORO staining objectified this observation, and a significant reduction in lipid droplets number and total droplet surface was observed in the TriMetChalc-treated group compared to the control (Figure 7C,D). The size of the lipid droplet remained unchanged (Figure 7E).

To enable a thorough understanding of the effect of TriMetChalc on MAFLD known to develop in the *ob/ob* model, a lipidomic analysis of liver was performed [16,17]. The results are expressed in relative abundance of each compound as an area ratio between the area of the detected species and the area of the internal standard normalized per mg of proteins in the sample. We firstly quantify liver content of cholesterol and triacyglycerols (TAG). Despite a clear downward trend towards lower concentrations in both cholesterol and TAG, no significant difference could be demonstrated with the sampling and the administration protocol used (Figure 8A–C and Table 1).

Fatty acids (FA) constitute the fundamental structural components of complex lipids and can enter the system through dietary intake, are released from visceral adipose tissue during lipolysis, or are synthesized within the liver through *de novo* lipogenesis (DNL). Considering the consistent association between hepatic steatosis and saturated (SFA), monounsaturated (MUFA), and polyunsaturated (PUFA) fatty acids, an investigation of their levels across the studied groups was performed. Analysis of FA contents within the liver of control and TriMetChalc (65 mg/kg BW)-treated mice revealed a significant reduction of total FA (Figure 9A and Table 2). Regarding SFA, a clear reduction of total SFA was observed in *ob/ob* mice that received TriMetChalc (Figure 9B and Table 2). Palmitic acid (FA C16:0) and stearic acid (FA C18:0) were the most prevalent SFA in liver samples from *ob/ob* mice and their abundance was reduced by TriMetChalc treatment (Figure 9C,D and Table 2). MUFAs including palmitoleic acid (FA C16:1), oleic acid (FA C18:1) and eicosenoic acid (FA C20:1) were found to be significantly reduced by TriMetChalc administration (Figure 9E–H and Table 2). Concerning PUFAs, linoleic acid (FA C18:2n6) and alpha-linolenic acid (FA C18:3n3) were found increased after TriMetChalc treatment (Table 2). Accordingly, total conjugated linoleic acid (CLA-FA) and total PUFAs contents exhibited an increase in the TriMetChalc group (Figure 9I,J and Table 2). Altogether these results contributed to an increase of PUFA/SFA and USFA/SFA ratio and a reduction of MUFA/PUFA ratio (Figure 9K and Table 2). The lipogenic index derived from the ratio of palmitic acid (FA C16:0) to the essential ω-6 linoleic acid (FA C18:2n6) reflects rates of DNL. Here we reported a strong reduction in the lipogenic index: 8.20 +/- 0.66 versus 3.24 +/- 0.73 in control and TriMetChalc-treated mice respectively (Figure 9L and Table 2). We next evaluated liver phospholipids, ceramides and sphingomyelins contents in control and treated groups. Interestingly, phosphatidylcholines (PCs) and phosphatidyl inositols (PI) were weakened by the treatment while phosphatidyl-ethanolamines (PE) and phosphatidyl serines (PS) levels was not significantly reduced despite to trend toward lower concentrations (Figure 10A–D and Table 3). As a result, the PC/PE ratio was significantly reduced (32.5 +/- 0.9 versus 29.2 +/- 0.7, P 0.01) in control and TriMetChalc-treated groups respectively, Figure 10E). Ceramides and sphingomyelins contents remained unchanged by TriMetChalc treatment (Table S1).
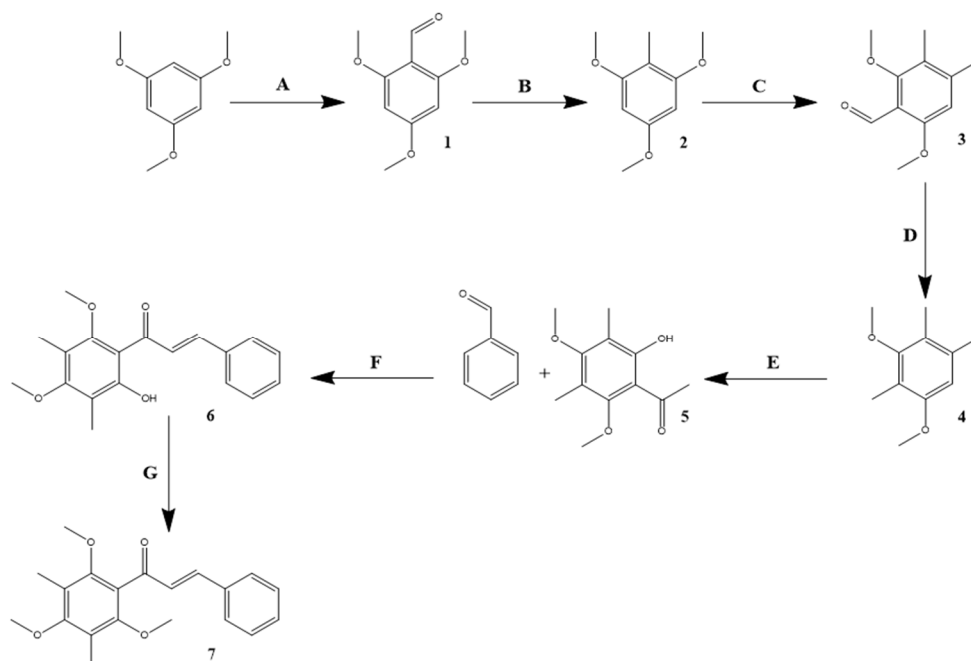
2.6. Figures, Tables and Schemes

Figure 1. Synthesis path to obtain 3,5-dimethyl-2,4,6-trimethoxychalcone (TriMetChalc). **A**: dimethylformamide, phosphorous oxychloride, 0° C, 1h. **B**: hydrazine hydrate, KOH, ethylene glycol 90-145 °C, 4h. **C**: dimethylformamide, phosphorous oxychloride, 0° C, 1h. **D**: hydrazine hydrate, KOH, ethylene glycol 90-145 °C, 4h. **E**: boron trifluoride ethyl etherate, acetic anhydride, 90 °C, 1.5h. **F**: LiOH, ethanol, 25 °C, 16h. **G**: K_2CO_3, dimethyl sulfate, acetone, 50 °C, 12h.
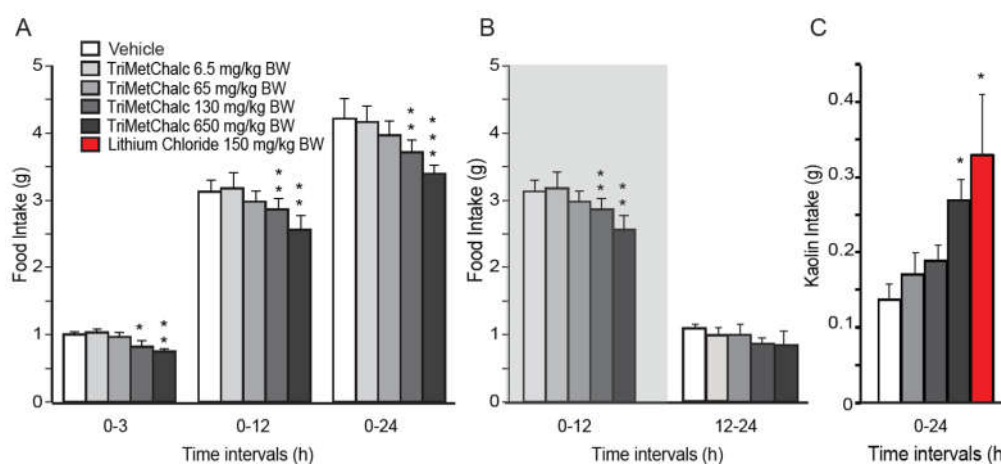

Figure 2. TriMetChalc reduced Food Intake. (A–B) Cumulative food intake measured over a 24 h period in C57Bl/6J mice *per os* administered with vehicle or TriMetChalc (6.5 to 650 mg/kg BW). In B, the dark period is represented by a shaded box. *$p < 0.05$, **$p < 0.01$, ***$p < 0.001$, significantly different from vehicle-treated mice. (C) Kaolin intake measured in C57Bl/6 mice 24 h after vehicle, TriMetChalc (65 to 650 mg/kg BW) or LiCl (150 mg/kg BW) administration. *$p < 0.05$ and significant difference from vehicle-treated mice.
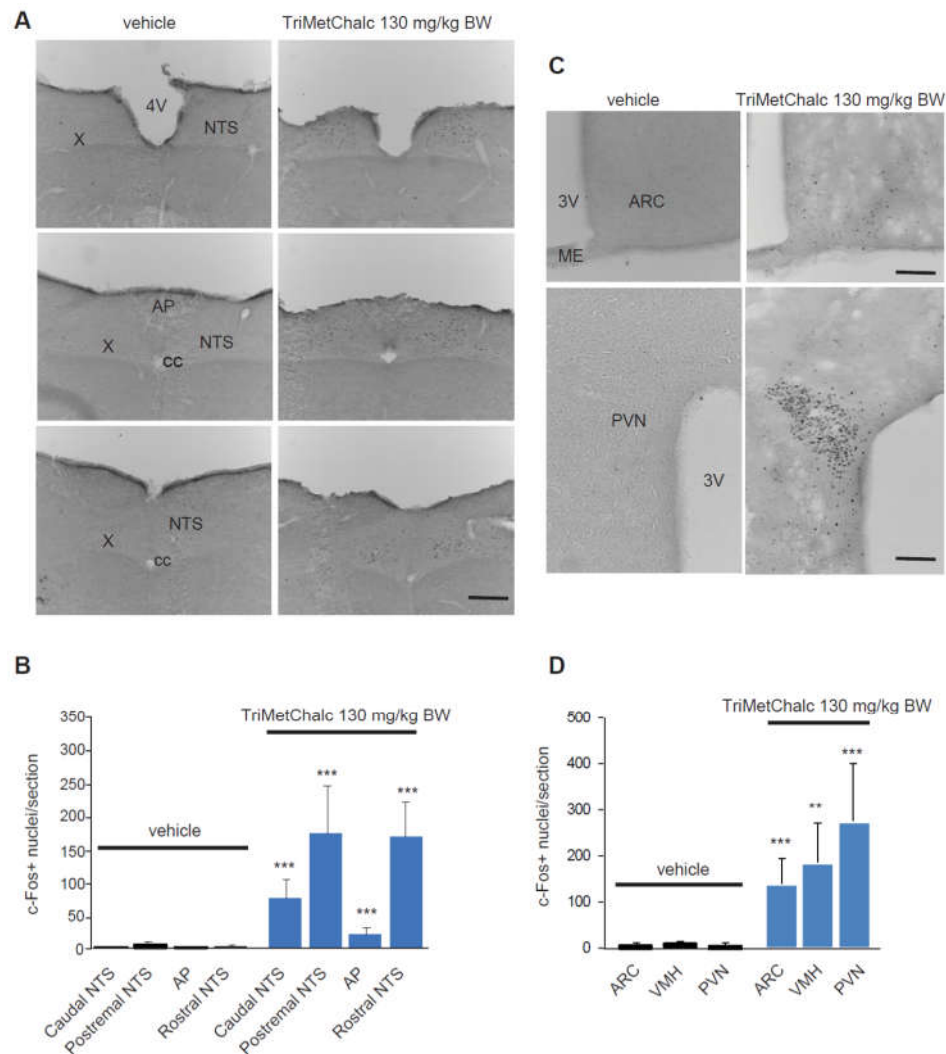
Figure 3. Identification of TriMetChalc-sensitive brain structures in C57Bl/6J mice. (A-C) Representative coronal sections illustrating the c-Fos labeling observed within brainstem (A) and hypothalamic (C) regions of C57Bl/6J mice treated with vehicle (left panel) or animals sacrificed 3 h (right panel) after *per os* treatment with TriMetChalc (130 mg/kg BW). Scale bar: 200 μm. (B-D) Quantification of the number of c-Fos-immunoreactive nuclei observed within the brainstem (B) and hypothalamic (D) structures 3 h after treatment with either vehicle or TriMetChalc (130 mg/kg BW). **$p < 0.01$, ***$p < 0.001$ significantly different from vehicle-treated mice. AP, area postrema; ARC, arcuate nucleus; cc, central canal; ME, median eminence; NTS, nucleus tractus solitarii; PVN, paraventricular nucleus; VMH: ventromedial hypothalamus; X, dorsal motor nucleus of the vagus nerve; 3V, third ventricle; 4, fourth ventricle.
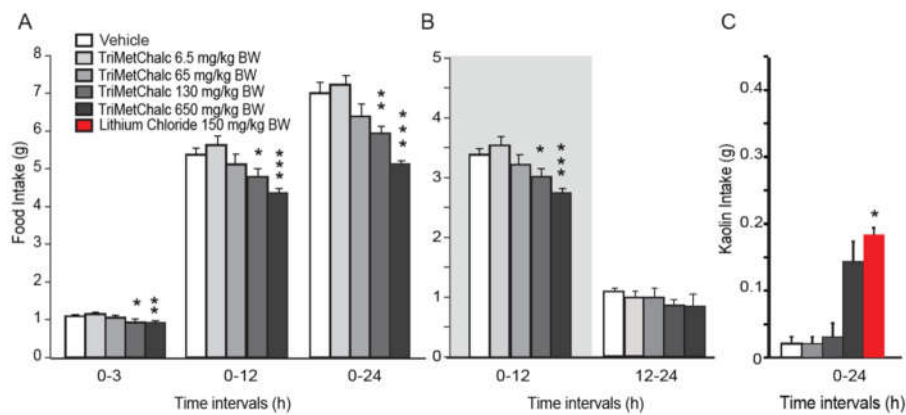
Figure 4. TriMetChalc reduced Food Intake in *ob/ob* mice. (A–B) Cumulative food intake measured over a 24 h period in *ob/ob* mice *per os* administered with vehicle or TriMetChalc (6.5 to 650 mg/kg BW). In B, the dark period is represented by a shaded box. *$p < 0.05$, **$p < 0.01$, ***$p < 0.001$, significantly different from vehicle-treated mice. (C) Kaolin intake measured in *ob/ob* mice 24 h after vehicle, TriMetChalc (65 to 650 mg/kg BW) or LiCl (150 mg/kg BW) administration. *$p < 0.05$ significant difference from vehicle-treated mice.
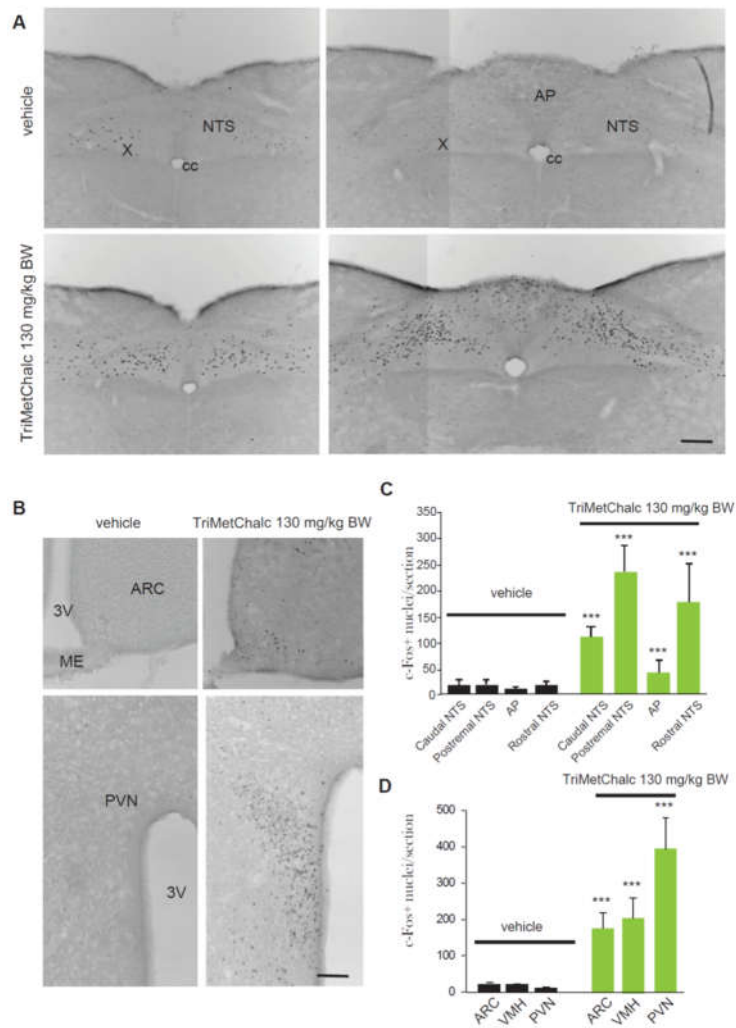

Figure 5. Identification of TriMetChalc-sensitive brain structures in *ob/ob* mice. (A-B) Representative coronal sections illustrating the c-Fos labeling observed within brainstem (A) and hypothalamic (B) regions of *ob/ob* mice treated with vehicle or animals sacrificed 3 h after treatment with TriMetChalc (130 mg/kg BW). Scale bar: 200 μm. (C-D) Quantification of the number of c-Fos-immunoreactive

nuclei observed within the brainstem (C) and hypothalamic (D) structures 3 h after treatment with either vehicle or TriMetChalc (130 mg/kg BW). ***$p < 0.001$, significantly different from vehicle-treated mice. AP, area postrema; ARC, arcuate nucleus; cc, central canal; ME, median eminence; NTS, nucleus tractus solitarii; PVN, paraventricular nucleus; VMH: ventromedial hypothalamus; X, dorsal motor nucleus of the vagus nerve; 3V, third ventricle.
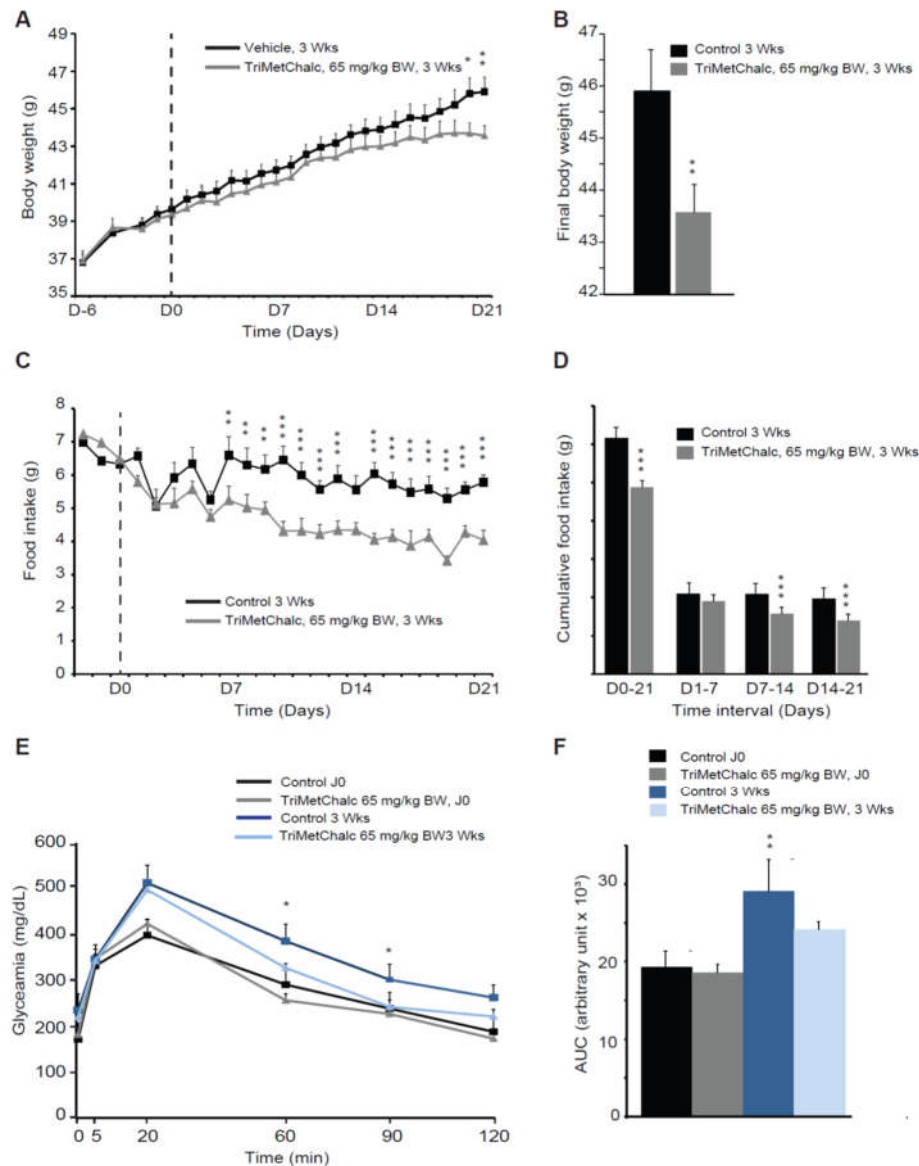

Figure 6. Chronic TriMetChalc administration reduces leptin dependent obesity. (A) Body weight measured from day 0 to 21 after *per os* administration of either saline or TriMetChalc (65 mg/kg BW) in *ob/ob* mice. The dashed line indicates the first day of treatment. (B) Final body weight measured on day 21 after *per os* administration of vehicle or TriMetChalc (65 mg/kg BW) in *ob/ob* mice. *$p < 0.05$, **$p < 0.01$, significantly different from vehicle-treated mice. (C-D) Daily food intake (C) and cumulative food intake (D) measured from day 0 to 21 following administration of either vehicle or TriMetChalc (65 mg/kg BW) in ob/ob mice **$p < 0.01$, ***$p < 0.001$ significantly different from vehicle-treated mice. (E) Oral glucose tolerance test using *per os* glucose administration (1.5 g/kg) performed before and after a 21-day period of vehicle or TriMetChalc (65 mg/kg BW) administration in *ob/ob* mice. (F) Quantification of area under the curves (AUC) measured at 120 min after *per os* glucose administration., significantly different from vehicle-treated mice.
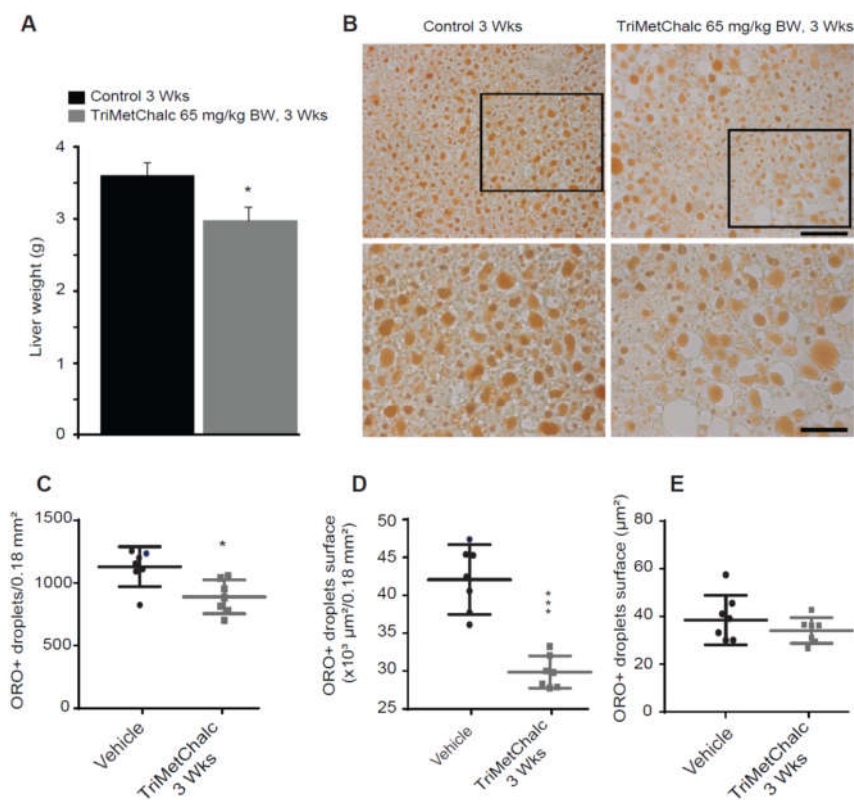
Figure 7. Chronic TriMetChalc administration ameliorates liver steatosis in *ob/ob* mice. (A) Liver weight measured in control and TriMetChalc (65 mg/kg BW) groups at the end of the treatment period. (B) Representative photomicrographs of ORO staining observed in vehicle- and TriMetChalc (65 mg/kg BW)-treated *ob/ob* mice. Black boxes (upper panels) indicate where high magnification images (lower panels) originated. (C-E) Quantification of ORO+ inclusion number per surface unit (C), total surface covered by ORO+ inclusions (D) and mean surface of ORO+ inclusion (E) in liver of vehicle- and TriMetChalc (65 mg/kg BW)-treated mice. * $P < 0.05$, *** $P < 0.001$, significantly different from vehicle-treated mice. Scale bar: 10 μm.
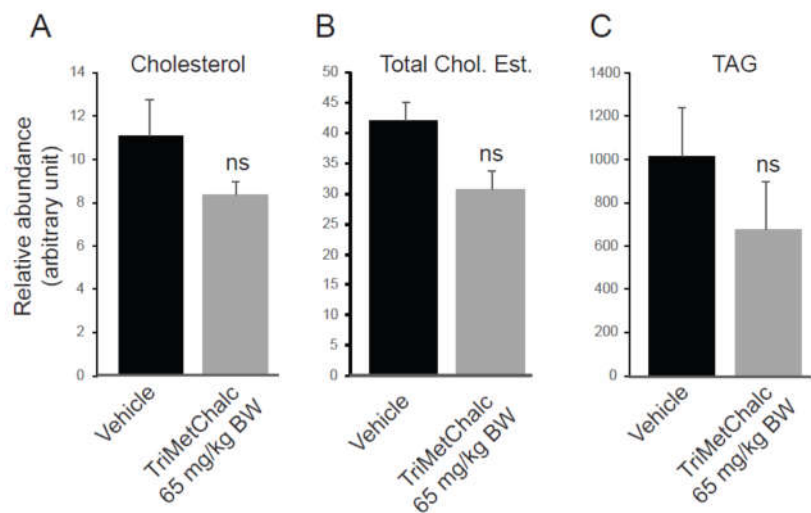

Figure 8. Quantification of free cholesterol (A), cholesterol ester (B) and triacylglycerols (C) on liver extracts from vehicle or TriMetChalc (65 mg/kg BW) treated *ob/ob* mice. ns: non-significant difference.
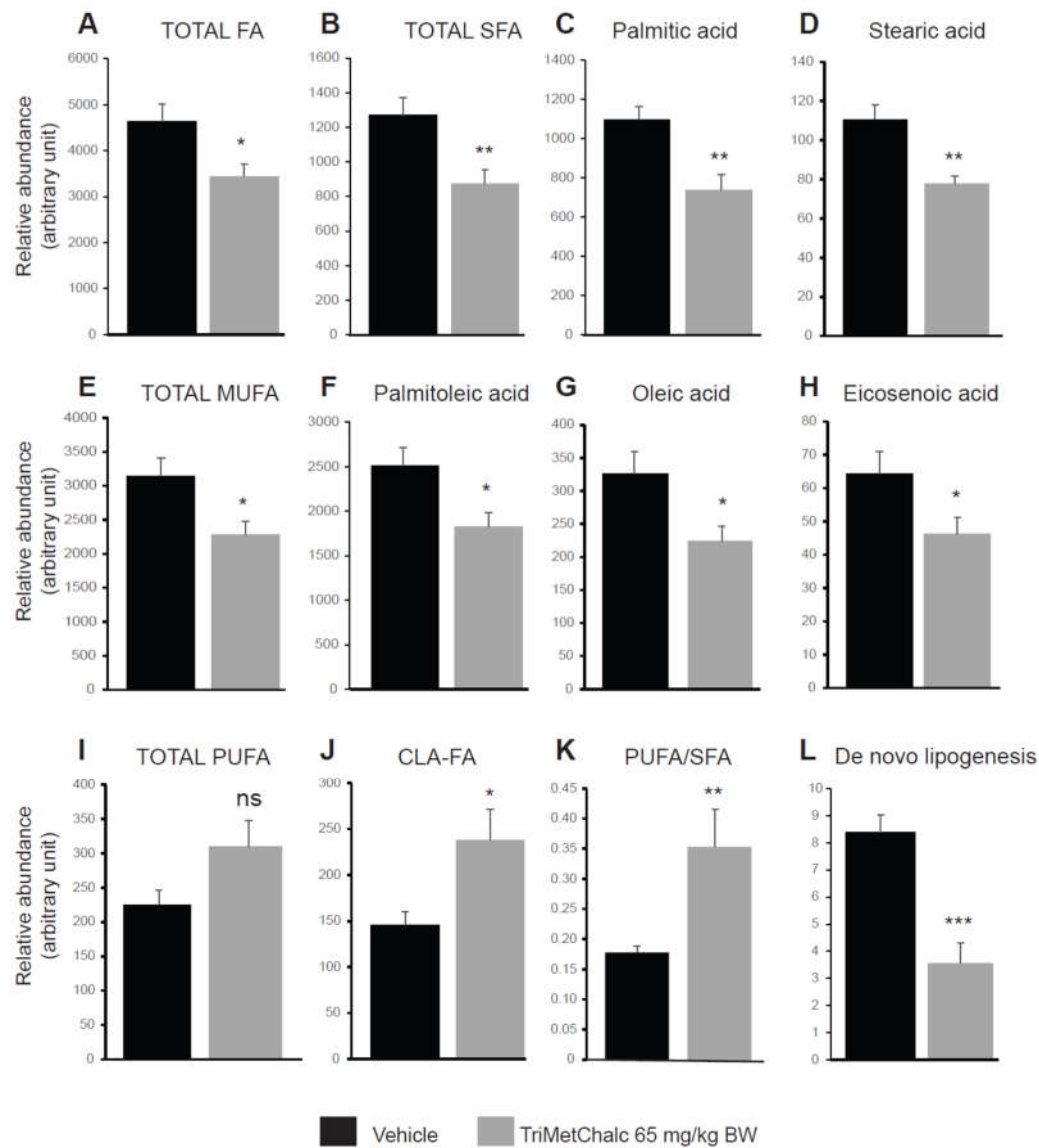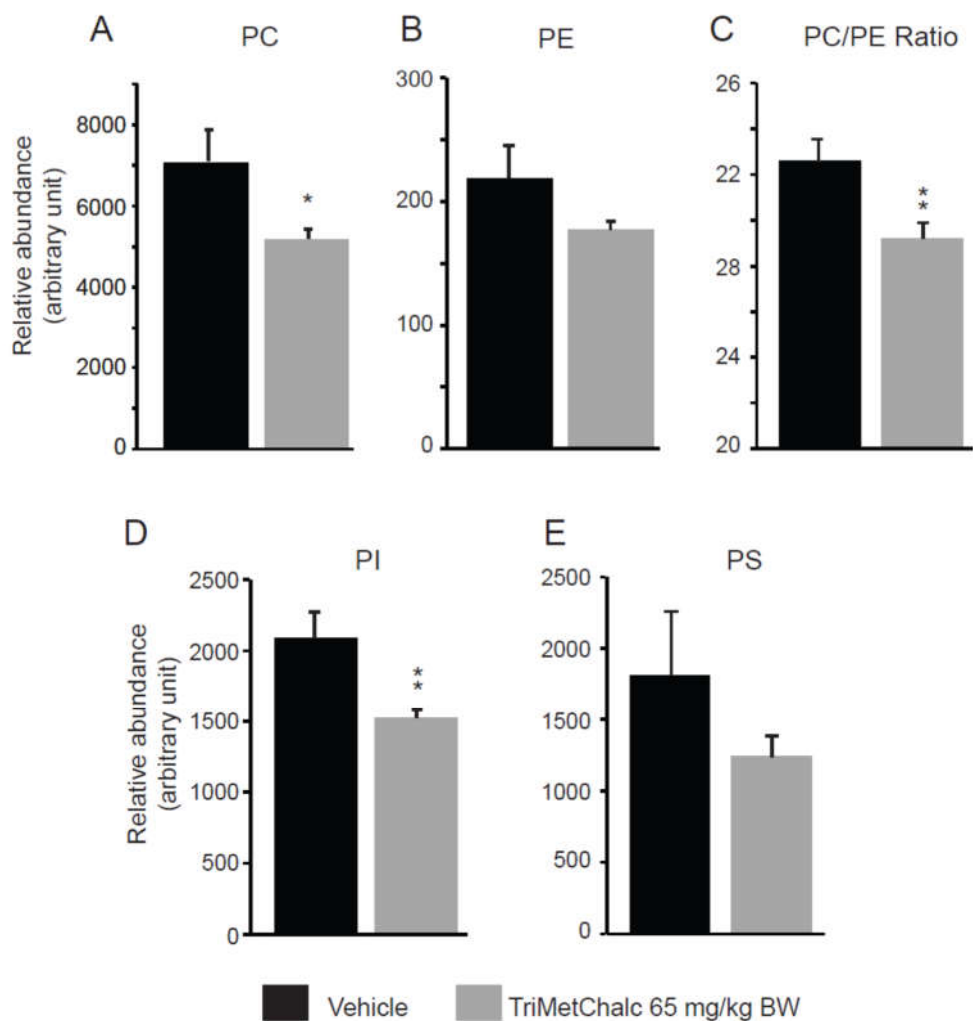
Figure 9. Quantification of FA (A), SFA (B-D), MUFA (E-H) and PUFA (I-J) on liver extracts from vehicle or TriMetChalc (65 mg/kg BW) treated *ob/ob* mice. PUFA/SFA ratio (K) and de novo lipogenesis (L) were calculated from data detailed within Table 2. * $P < 0.05$, **$p < 0.01$, ***$p < 0.001$ significantly different from vehicle-treated mice, ns: non-significant difference.

Figure 10. Quantification of phosphatidylcholines (PC, A), phosphatidylethanolamines (PE, B), PC/PE ratio (C), phosphatidylinositols (PI, D) and phosphatidylserines (PS, E) on liver extracts from vehicle or TriMetChalc (65 mg/kg BW) treated *ob/ob* mice. * $P < 0.05$, ** $p < 0.01$ significantly different from vehicle-treated mice, ns: non-significant difference.

	Vehicle		TriMetChalc 65 mg/kg		Vehicle *vs* TriMetChalc
	Moy	SEM	Moy	SEM	T Test
L_Cholesterol	11.08	1.67	8.37	0.59	0.15
L_Chol_C16	14.86	2.25	10.84	1.14	0.14
L_Chol_C18	25.45	3.88	18.66	1.79	0.14
L_Chol_C20	1.74	0.16	1.21	0.20	0.07
Total Chol Est	42.05	6.18	30.72	3.03	0.13
L_TAG46	nd	-	nd	-	-
L_TAG48	37.36	12.61	25.17	11.45	0.49
L_TAG50	228.96	83.53	154.07	63.95	0.49
L_TAG52	535.88	200.02	361.51	120.48	0.47
L_TAG54	191.14	79.43	119.89	25.80	0.41
L_TAG56	22.58	7.56	14.68	2.03	0.33
Total TAG	1015.94	382.54	675.34	223.35	0.45
LN Totaux	1069.08	389.9	714.45	221.14	0.44

Table 1. Detailed cholesterol and triacylglycerols composition and quantification of liver extracts from vehicle or TriMetChalc (65 mg/kg BW) treated *ob/ob* mice.

Fatty Acids	Vehicle		TriMetChalc 65 mg/kg		Vehicle *vs* TriMetChalc
	Moy	SEM	Moy	SEM	T Test
TOTAL FA	4641.43	382.72	3444.58	264.42	0.028
TOTAL SFA	1269.28	104.54	871.72	80.01	0.006
L_C14_0	12.29	1.35	10.44	1.73	0.417
L_C15_0	1.35	0.22	1.10	0.09	0.332
L_C16_0	1098.45	92.91	739.88	76.59	0.014
L_C17_0	2.42	0.39	1.64	0.11	0.083
L_C18_0	110.73	11.19	77.74	3.77	0.019
L_C20_0	1.20	0.12	1.04	0.12	0.406
L_C21_0	nd	nd	nd	nd	nd
L_C22_0	nd	nd	nd	nd	nd
L_C23_0	nd	nd	nd	nd	nd
L_C24_0	42.84	3.67	40.05	5.45	0.680
TOTAL MUFA	3147.66	263.23	2282.99	189.88	0.026
L_C14_1w7	0.54	0.09	0.40	0.08	0.300
L_C15_1w7	nd	nd	nd	nd	nd
L_C16_1w9	85.35	7.39	72.25	9.48	0.301
L_C16_1w7	160.64	12.72	110.38	10.01	0.011
L_C17_1w7	nd	nd	nd	nd	nd
L_C18:1w9	2508.61	210.06	1827.84	153,57	0.026
L_C18_1w7	326.27	33.31	228.08	32.08	0.030
L_C20_1w9	64.37	6.67	46.36	4.83	0.054
L_C22_1w9	1.88	0.21	1.52	0.27	0.326
L_C24_1w9	nd	nd	nd	nd	nd
TOTAL PUFA	224.50	21.88	310.39	37.52	0.084
L_C16_2w6	nd	nd	nd	nd	nd
L_C16_2w4	nd	nd	nd	nd	nd
L_C16_3	4.20	0.60	2.75	0.25	0.051
L_C16_4w3	nd	nd	nd	nd	nd
L_C18_2w6	141.41	14.77	228.50	23.12	0.026
L_C18_3w6	1.55	0.14	1.64	0.17	0.692
L_C18_3w3	2.84	0.40	4.95	0.97	0.050
L_C18_4w3	nd	nd	nd	nd	nd
L_C20_2w6	8.86	0.96	3.24	0.79	0.001
L_C20_3w3	nd	nd	nd	nd	nd
L_C20_3w6	12.74	1.39	11.23	0.73	0.357
L_C20_4w6	40.97	3.78	39.92	3.56	0.844
L_C20_5w3	2.19	0.27	2.45	0.59	0.694
L_C22_2w6	3.09	0,46	1.72	0.37	0.043
L_C22_3w3	nd	nd	nd	nd	nd
L_C22_4w6	2.30	0.30	2.70	0.22	0.307
L_C22_5w3	4.36	0.91	5.31	0.91	0.478
L_C22_6w3	nd	nd	nd	nd	nd
MUFA/PUFA	14.19	0.83	8.61	1.35	0.006
MUFA/SAFA	2.48	0.05	2.64	0.08	0.141
PUFA/SAFA	0.18	0.01	0.35	0.06	0.019
USFA/SAFA	2.66	0.05	2.99	0.13	0.041
DNL	8.20	0.66	3.24	0.73	0.001

Table 2. Detailed fatty acid (FA) composition and quantification of liver extracts from vehicle or TriMetChalc (65 mg/kg BW) treated *ob/ob* mice.

	Vehicle		TriMetChalc 65 mg/kg		CT vs TriMetChalc
	Moy	SEM	Moy	SEM	*T Test*
Total PC	7057.94	757.8	5187.62	281.29	0.04
L_PC28_0	0.09	0.01	0.06	0.005	0.04
L_PC30_0	7.32	0.63	6.01	0.59	0.16
L_PC30_1	0.77	0.08	0.5	0.06	0.03
L_PC32_0	279.32	18.77	249.1	25.07	0.35
L_PC32_1	123.51	17.61	76.98	10.96	0.04
L_PC32_2	8.08	0.88	5.52	0.63	0.04
L_PC34_0	187.36	18.73	125.08	12.102	0.01
L_PC34_1	1673.29	187.02	1065.24	111.26	0.01
L_PC34_2	507.53	64.06	468.49	29.59	0.59
L_PC34_3	28.72	2.31	26.75	1.49	0.49
L_PC36_1	525.28	50.46	294.9	38.24	0.001
L_PC36_2	693.58	81.86	514.46	20.31	0.05
L_PC36_3	487.84	54.12	369.98	14.4	0.06
L_PC36_4	490.33	50.25	475.27	28.86	0.8
L_PC38_2	69.62	8.11	37.29	4.99	0.001
L_PC38_3	104.89	13.74	54.43	7.37	0.001
L_PC38_4	579.10	64.85	484.69	36.01	0.23
L_PC38_5	318.35	27.7	258.8	11.99	0.07
L_PC38_6	574.35	68.66	418.17	14.18	0.05
L_PC40_3	3.29	0.43	2.03	0.24	0.02
L_PC40_6	395.25	58.66	253.76	18.78	0.04
Total PE	218.77	26.68	177.54	8.19	0.17
L_PE32_0	0.51	0.05	0.39	0.01	0.15
L_PE32_1	0.55	0.06	0.34	0.05	0.03
L_PE32_2	0.03	0,00	0.04	0,00	0.23
L_PE34_0	7.67	0.87	5.77	0.51	0.08
L_PE34_1	4.03	0.60	3.57	0.14	0.47
L_PE36_1	11.03	1.32	8.18	0.38	0.06
L_PE36_2	11.59	1.70	9.07	0.35	0.17
L_PE36_3	11.47	1.60	9.70	0.40	0.30
L_PE36_4	11.08	1.36	9.62	0.56	0.34
L_PE38_2	4.05	0.5	2.80	0.17	0.04
L_PE38_3	28,00	3.39	24.3	1.30	0.33
L_PE38_4	37.77	3.93	34.615	1.76	0.48
L_PE38_5	22.67	2.93	16.21	1.00	0.06
L_PE38_6	23.28	2.86	18.88	1.02	0.17
L_PE40_3	0.67	0.06	0.64	0.04	0.68
L_PE40_5	14.94	2.25	10.3	0.59	0.07
L_PE40_6	21.71	2.85	15.86	0.85	0.07
L_PE40_7	7.64	0.67	7.179	0.32	0.53
Total PI	2088.61	184.57	1519.7	52.79	0.01
L_PI32_1	1.96	0.22	2.37	0.23	0.22
L_PI34_1	6.48	0.501	5.02	0.57	0.08
L_PI34_2	4.59	0.26	4.15	0.11	0.16
L_PI36_0	3.57	0.34	2.8	0.26	0.10
L_PI36_1	14.15	1.24	9.31	0.99	0.01
L_PI36_2	28.07	2.25	18.5	1.12	0.003
L_PI36_3	46.02	3.99	28.61	1.98	0.002
L_PI38_1	11.12	1.20	5.22	0.79	0.002
L_PI38_2	141.16	14.94	61.32	8.51	0.001
L_PI38_3	648.17	61.76	399.12	19.19	0.003
L_PI38_4	955.97	85.72	802.87	39.00	0.13
L_PI38_5	153.26	12.2	126.5	5.12	0.07
L_PI40_2	9.01	1.25	8.67	0.60	0.81
L_PI40_3	11.97	1.15	7.46	0.56	0.005
L_PI40_4	18.32	1.53	11.75	1.13	0.006
L_PI40_5	19.03	1.08	13.45	0.53	0.001
L_PI40_6	15.68	0.71	12.49	0.68	0.01

	Vehicle		TriMetChalc 65 mg/kg		CT vs TriMetChalc
	Moy	SEM	Moy	SEM	T Test
Total PS	1814.09	445.13	1240.94	149.90	0.29
L_PS32_0	14.02	1.87	12.03	1.92	0.51
L_PS32_1	nd	-	nd	-	-
L_PS34_0	10.85	1.37	9.38	0.90	0.43
L_PS34_1	25.7	5.80	17.53	2.74	0.27
L_PS34_2	5.34	0.99	4.68	0.33	0.57
L_PS36_0	25.07	5.99	15.81	1.64	0.20
L_PS36_1	135.34	33.58	83.18	10.02	0.20
L_PS36_2	36.59	8.88	24.74	2.80	0.27
L_PS36_3	15.77	3.40	13.08	1.39	0.51
L_PS38_1	nd	-	nd	-	-
L_PS38_2	30.13	7.79	16.93	1.85	0.16
L_PS38_3	162.72	42.46	107.88	14.12	0.28
L_PS38_4	570.09	135.58	449.79	52.49	0.46
L_PS38_6	72.86	15.55	63.68	6.51	0.63
L_PS40_4	44.63	11.28	29.62	4.31	0.28
L_PS40_5	140.837	37.33	81.48	11.44	0.19
L_PS40_6	524.08	135.80	311.08	47.10	0.20
L_PS42_6	nd	-	nd	-	-

Table 3. Detailed phospholipids composition and quantification of liver extracts from vehicle or TriMetChalc (65 mg/kg BW) treated *ob/ob* mice.

3. Discussion

The present study was designed to evaluate the potential therapeutic effects of TriMetChalc on food intake, obesity and liver steatosis using the hyperphagic, obese and diabetic *ob/ob* mice model. We observed that TriMetChalc which derived from DMC retained the anti-obesity and anti-diabetic effects of the native molecule but we also showed that this molecule has an anorexigenic property and protective action on the liver, two actions which have not been described for DMC.

3.1. TriMetChalc Acts as Anorexigenic Molecule Independently of Leptin

Per os administration of TriMetChalc induced a dose-dependent reduction in daily food intake by decreasing night-time food consumption. This result proves that TriMetChalc was stable and effective in vivo after daily administration. An interesting finding of the present work is that the anorexigenic effect of TriMetChalc was similar in C56Bl/6 and leptin-deficient *ob/ob* mice. Leptin is a hormone secreted by adipose cells that inhibits hunger. Leptin-deficient *ob/ob* mice are hyperphagic and develop severe obesity, insulin resistance, and steatosis. Therefore, TriMetChalc acts on leptin-independent signaling pathways or molecular targets operating downstream of leptin. Thus, the anorexigenic action of TriMetChalc in *ob/ob* mice is of interest in the perspective of the future development of TriMetChalc as an anti-obesity drug since human obesity is characterized by leptin resistance [18]. The reduction in food intake may be the result of intoxication and the appearance of nausea and vomiting [19]. To verify whether this was the case with TriMetChalc, we measured the consumption of the clay (kaolin) intake, used here as an indicator of nausea and emesis [20]. The dose of 130 mg/kg BW, which induces a reduction in food intake, did not lead to any kaolin consumption, excluding the presence of nausea at this dosage. On the other hand, at a high dose, i.e., 650 mg/kg BW, TriMetChalc significantly increases the ingestion of kaolin, showing that a high dosage of this molecule is likely to induce discomfort in animals. In terms of toxicity, we did not observe any remarkable histological liver damage after administration of TriMetChalc for 3 weeks. In addition, the results of the single-dose acute-toxicity study showed no toxicity or abnormal clinical signs in the mice. The estimated LD 50 is higher than 1300 mg/kg, which is much higher than the effective dosage (6.25 and 650 mg/kg) administered to the mice in this study. Taken together, the TriMetChalc compound demonstrated no significant toxicity at the doses used in the present work.

By controlling hunger, the brain plays an essential role in regulating food intake and energy expenditure. Two central regions, i.e., the hypothalamus and dorsal vagal complex (DVC), a brainstem structure, strongly contribute to the homeostatic control of the energy balance by integrating information linked to nutritional status and arising from peripheral organs (gut, liver, pancreas, adipose tissue; see [21] for review). To decipher the mechanisms underlying the modulation of food intake by TriMetChalc and identify central structures activated by this compound, we performed a c-Fos expression mapping. The detection of the early gene c-Fos is classically used to identify brain-activated cells [22,23]. We observed that TriMetChalc strongly and specifically activated hypothalamic nuclei such as ARC, PVN, VMH, and the brainstem nuclei of the DVC. It should be noted that TriMetChalc did not cause c-Fos activation outside these areas, excluding a nonspecific toxic effect. On the contrary, the specific activation of these areas reinforces the idea that the TriMetChalc interacts with pathways dedicated to the regulation of food intake. As mentioned previously, TriMetChalc is a derivative of DMC, the major compound in *Cleistocalyx operculatus* extract. Choi and colleagues [12] reported that DMC activated AMP-activated protein kinase (AMPK) by direct binding and proposed that DMC is an AMPK agonist. AMPK was highly expressed in the different hypothalamic nuclei, such as ARC, PVN, and VMH [24]. Hypothalamic AMPK is involved in the modulation of energy balance and plays an important role in the regulation of feeding. The modulation of hypothalamic AMPK level and activity by key hormones such as leptin and ghrelin is implicated in the control of food intake and appetite [25]. For example, during fasting, AMPK activity is raised in hypothalamus nuclei, and it is inhibited after refeeding. Furthermore, elevated hypothalamic AMPK activity caused increased food intake leading to weight gain. Conversely, hypophagia and weight loss were caused by its suppression [26]. Thus, given the anorexigenic effect observed here with TriMetChalc, it seems unlikely that it acts as a hypothalamic AMPK agonist. We showed here that TriMetChalc limited the weight gain of *ob/ob* mice over a period of three weeks, a duration similar to that used in the two previously cited studies [12,27]. Three weeks of DMC treatment improved glucose tolerance in HFD-induced obese mice but the body weight of DMC-treated mice remains unchanged compared with that of the control group [12]. Recently, Lee and collaborators [27] synthesized 12 chalcone derivatives from DMC possessing AMPK agonist activity. These derivatives increased the fatty acid oxidation (FAO) rate of C2C12 myotubes. After three weeks of administration, the more potent effective AMPK agonist derivate was reported to improve glucose tolerance in HFD-mice without modification in weight gain [27]. In addition, we revealed that TriMetChalc reduces food intake from the 7th day until the end of treatment. As a result, cumulative food intake over the 3-week period was reduced. This is a notable difference from the works of Choi et al. [12] and Lee et al. [27], which suggests that modifying DMC as we practiced it allows the molecule to have an anorexigenic effect. Other synthetic chalcones derivatives, i.e., halogen-containing chalcone derivatives 2-bromo-4′-methoxychalcone and 2-iodo-4′-methoxychalcone, have been reported to prevent body weight gain and impaired glucose tolerance in HFD mice after 10 weeks of treatment [28]. But in the absence of measurement of food intake in this latest study, it is difficult to compare the effects of these different molecules. To date, our work is the first to show that a chalcone derivative has a hunger-killing effect by directly or indirectly targeting neural networks dedicated to the central energy balance. Understanding the precise mechanism remains to be clarified.

3.2. TriMetChalc Attenuates Metabolic Dysfunction-Associated Fatty Liver Disease

Excess fat deposition within the liver has been reported for centuries. In 1980, Ludwig and colleagues describe the liver histology associated with excess liver fat in the absence of significant alcohol consumption and use the term "non-alcoholic steatohepatitis (NASH)" [29]. Non-alcoholic fatty liver disease (NAFLD) is rapidly becoming a worldwide public health problem. NAFLD represents a spectrum of diseases ranging from "simple steatosis," which is considered relatively benign, to non-alcoholic steatohepatitis (NASH) and NAFLD-associated cirrhosis and end-stage liver disease. Even if NAFLD can be induced by a variety of drugs and toxins, a high prevalence of NAFLD in patients with obesity, metabolic syndrome, and type-2 diabetes was clearly observed [30]. In 2020,

to better reflect the metabolism-related etiology, an international panel of experts reached a consensus to replace the term NAFLD with "metabolic dysfunction-associated fatty liver disease" (MAFLD) [4,5]. In addition to obesity and type 2 diabetes, *ob/ob* mice develop steatosis and associated lipotoxicity and lipo-apoptosis. Liver histology shows a rare progression to cirrhosis since *ob/ob* mice are resistant to hepatic fibrosis. Although *ob/ob* mice do not display the full spectrum of human NASH, these obese animals could represent a suitable model to study MAFLD [16].

Numerous chalcones, i.e., trans-chalcone, naringenin chalcone, xanthohumol, 4-hydroxyderricin, xanthoangelol, cardamonin, flavokawain B, and safflower yellow, have been shown to have protective effects on the liver and in MAFLD. To do this, they can improve adipocyte functions, increase adiponectin secretion, inhibit lipogenesis, or enhance fatty acid oxidation (see [9] for review). However, no such effects have been reported for DMC. Only one study shows that DMC has a hepatoprotective effect on carbon tetrachloride-induced acute liver injury in Kunming mice through the attenuation of oxidative stress and inhibition of lipid peroxidation [31]. Here, we observed that treatment for three weeks with a dose of 65 mg/kg BW of TriMetChalc significantly reduced hepatic steatosis in *ob/ob* mice, as quantified by histological staining. This is the first observation that a DMC derivative compound can have a positive impact on this pathology. An important aspect of MAFLD progression is lipotoxicity, caused by hepatic accumulation of lipids that can trigger cellular stress responses. We performed a lipidomic study to identify which lipids were modified by the treatment. Despite a trend towards a reduction in TAG and cholesterol, the quantification carried out here was unable to highlight a significant difference. The three weeks exposure time may explain this result, and we will proceed with longer treatment periods in the future. We might also consider increasing the dose of TriMetChalc and/or combining TriMetChalc with other chalcones or compounds with liver-protective action. However, our protocol induced many modifications in long-chain FFAs (containing 16 carbons or more) divided into SFAs, MUFAs, and PUFAs based on the presence of double bonds. First, we observed a significant reduction in total SFAs content largely due to the decrease in palmitic and stearic acids. Increased levels of hepatic SFAs have been reported in MAFLD patients and animal models, largely due to significant increases in palmitic and stearic acids (see [32] for review). The excessive accumulation of these two SFAs in hepatocytes has been shown to induce endoplasmic reticulum stress, leading to apoptosis and hepatocyte damage. Hence, palmitic and stearic acids induce concentration- and time-dependent lipo-apoptosis in hepatocytes [33,34]. Palmitic acid through interaction with receptor toll-like type 2 has been shown to activate the inflammasome in Kupffer cells and macrophages *in vitro* and in vivo and then contribute to NASH development [35]. Conversely, the excessive SFA consumption may be a risk factor for MAFLD pathogenesis [36].

Animals and humans with MAFLD also have high levels of hepatic total MUFAs, suggesting a potential link between increased levels of these lipids and hepatic inflammation and lipotoxicity [37–39]. The most abundant and well-studied MUFAs in MAFLD are palmitoleic acid (C16:1) and oleic acid (C18:1), which are generated from the SFAs palmitic and stearic acids, respectively [40]. Oleic acid-induced steatosis has been reported in hepatocytes of many mammalian species [41,42]. Although they contribute to steatosis, these MUFAs are less lipotoxic than SFAs. Indeed, individually studied, these MUFAs induce apoptosis, but this effect is minimal compared with SFAs [40]. Furthermore, they greatly attenuated palmitate-induced apoptosis in cultured hepatocytes [43]. Consistently, in cultured hepatocytes, MUFAs reduced palmitate-induced apoptosis but increased triglyceride (TAGs) accumulation [44]. Moreover, in a context of impaired TAGs synthesis, oleic acid accumulation exerts significant lipotoxicity [44]. Finally, the inhibition of stearoyl-CoA desaturase 1 (SCD1), a rate-limiting enzyme that allows the biosynthesis of monounsaturated fatty acids from their saturated fatty acid precursors, has been proposed as a treatment for MAFLD [45,46]. In this context, the concomitant decrease in SFAs and MUFAs, i.e., FA C16:0, FA C16:1, FA C18:0, FA C18:1, and FA C20:1, observed in TriMetChalc-treated *ob/ob* mice could help reduce lipotoxicity and TAGs accumulation.

Our lipidomic analyses revealed a significant increase in PUFAs contents, particularly linoleic acid (FA C18:2w6) and alpha-linolenic acid (FA C18:3w3). Accordingly, the PUFAs/SFAs ration was

found to be increased by TriMetChalc administration. In recent years, it has become clear that PUFAs are important for many biological processes within cells. For instance, PUFAs increase membrane fluidity, which raises the number of membrane insulin receptors and improves insulin sensitivity. Additionally, through their interactions with other genes, PUFAs directly regulate the activity of genes linked to lipid metabolism, redox balance, inflammation, and fibrogenesis in NASH (see [40,47] for reviews). The PUFAs content is altered in MAFLD, and the severity of this pathology is correlated with a constant decline in hepatic PUFAs levels. [38,48]. Thus, the molar percentages of both n-3 and n-6 PUFAs were decreased in human liver biopsies from MAFLD patients [38]. A low liver PUFAs/SFAs ratio has been associated with an increased risk of developing atherosclerosis, cardiovascular diseases, diabetes, and MAFLD [49]. In a meta-analysis, Yu and colleagues [50] found that total PUFAs improve liver function and promote benefits for obesity-related comorbidities, such as a reduction in insulin resistance, dyslipidemias, inflammation, and non-alcoholic fatty liver disease markers. PUFAs are effective at limiting the hepatic steatosis process by increasing the gene expression of lipid oxidation, reducing liver lipogenic enzymes activity, and releasing adiponectin [51]. The increase in PUFAs and the concomitant reduction in SFA and MUFA induced by TriMetChalc should be highlighted and could contribute to improve the liver status of the animals.

Liver steatosis in MAFLD is triggered by excessive hepatic triglyceride synthesis using white adipose tissue (WAT)-derived fatty acids, *de novo* lipogenesis (DNL), and endocytosis of triglyceride-rich lipoproteins. DNL, the metabolic pathway synthesizing SFAs and MUFAs from acetyl-CoA, accounts for only a small fraction of FAs in the liver of lean humans (5%) [3]. However, in MAFLD, hepatic DNL is strongly increased, and approximately 25% of triglycerides originate from DNL. This increase in MAFLD compared to healthy subjects can be largely explained by the induction of DNL enzymes [52]. The lipogenic index was introduced by Hudgins et al. in 1996 [53] to reflect the DNL rate and is calculated as the ratio of palmitic acid (16:0) to the essential omega-6 linoleic acid (18:2n6). The amounts of FA chains (i.e., FA C16:0, FA C18:0, and FA C18:1) representing DNL were substantially elevated in *ob/ob* mice [54]. Here, we reported a clear and strong reduction in the DNL index in response to TriMetChalc treatment, confirming the potential benefit of this molecule in the MAFLD context.

An interesting observation we made is the reduction of hepatic PC contents and PC/PE ratio with TriMetChalc treatment. PC and PE are the two most abundant phospholipids in the plasma membranes of all mammalian cells. PC and PE predominantly reside on the outer and inner leaflets of the plasma membrane bilayer, respectively. In the context of MAFLD, PC and PE have been associated to liver damage. In several mouse models and in human studies, a change not only in the absolute concentrations of these phospholipids but, more critically, in the molar ratio between PC and PE is a key determinant of liver health [55]. Mostly, the severity of MAFLD is generaly negatively correlated with the hepatic PC/PE ratio [56]. But in some models, the PC/PE ratio can be increased above the normal range, and this disturbance in the ratio is also associated with MAFLD. The leptin-deficient *ob/ob* mice belong to models where the hepatic PC/PE ratio is increased [57]. To manage excess lipids storage in these mice, the expression of genes involved in hepatic PC synthesis (i.e., Pcyt1a and Pemt) is up-regulated, increasing the hepatic PC/PE ratio [58]. When *ob/ob* mice were treated with Pemt-targeted shRNA, the hepatic PC/PE molar ratio was restored to the wild-type level, thereby significantly decreasing hepatic steatosis [55]. In this context, the reduction in PC/PE ratio observed in response to TriMetChalc could contribute to the reduction of liver steatosis in this model and be an indicator of the improvement in the metabolic status of the *ob/ob* mice.

4. Materials and Methods

4.1. Animal Housing

Experiments were performed on 7-8 weeks male C57Bl/6J mice and homozygous male C57BL/6J-*lep*[ob] (*ob/ob*) mice (Charles River Laboratories, l'Abresle, France). All animals were individually housed in a pathogen-free facility at controlled temperature on a 12/12 h light/dark cycle (lights on at

7 AM) with standard diet (AO4 P2.5, SAFE UAR) and water available *ad libitum*. All experiments were performed at 21°C. Each experimental group comprised 8 animals.

4.2. 3,5-dimethyl-2,4,6-trimethoxychalcone (TriMetChalc) Synthesis Pathway (Figure 1)

4.2.1. Synthesis of 2,4,6-trimethoxybenzaldehyde

According to a previously described synthesis [59,60], 15 g of 1,3,5-trimethoxybenzene were dissolved in 9 mL of dimethylformamide (1.3 equimolar (eq.)) and cooled at 0 °C. A volume of 9.1 ml of phosphorous oxychloride (1.1 eq) was slowly added dropwise and the mixture was allowed to react at room temperature for 1h. After completion, the mixture was cooled with ice cold water and neutralized with 8M KOH. The precipitate was filtered, and a pink solid was obtained (93% yield). ^{1}H NMR (300MHz, DMSO-d_6): δ 10.19 (s, 1H, CHO), 6.23 (s, 2H, CH), 3.86 (s, 3H, O-CH$_3$), 3.81 (s, 6H, O-CH$_3$).

4.2.2. Synthesis of 2,4,6-trimethoxytoluene

As described in a previous synthesis [59,60], 10 g of 2,4,6-trimethoxybenzaldehyde were dissolved in 30 mL of ethylene glycol. Then, 11.1 ml of hydrazine hydrate (0.5 eq.) and 14 g of KOH (5 eq.) were added. The solution was then heated to 90 °C for 2h, and once foam has formed, the mixture was heated to 145 °C for 2h. When completed, the reaction was poured on ice-cold water and acidified with 1M HCl. The precipitate was filtered and washed several times with brine to obtain a white powder (81% yield). ^{1}H NMR (300MHz, DMSO-d_6): δ 6.19 (s, 2H, CH), 3.74, (s, 9H, O-CH$_3$), 1.9 (s, 3H, CH$_3$)

4.2.3. Synthesis of 3-methyl-2,4,6-trimethoxybenzaldehyde

As for the previous formylation, 10g of 2,4,6-trimethoxytoluene were dissolved in 5.5 mLof dimethylformamide (1.3 eq.) and then cooled at 0 °C. Then, 5.6 mL of phosphorous oxychloride (1.1 eq.) were slowly added dropwise, and the mixture was allowed to react at room temperature for 1h. After completion, the mixture was cooled with ice cold water and neutralized with 8M KOH. The precipitate was filtered to obtain a bright yellow precipitate (89 % yield). ^{1}H NMR (300MHz, DMSO-d_6): δ 10.18 (s, 1H, CHO), 6.53 (s, 1H, CH), 3.91 (s, 3H, O-CH$_3$), 3.88 (s, 3H, O-CH$_3$), 3.68 (s, 3H, O-CH$_3$), 1.96 (s, 3H, CH$_3$)

4.2.4. Synthesis of 2,4-dimethyl-1,3,5-trimethoxybenzene

As for the previous reduction, 10 g of 3-methyl-2,4,6-trimethoxybenzaldehyde (0.05 mol) and 10.5 mL of hydrazine hydrate (0.6 equimolar) were dissolved in 30 mL of ethylene glycol. When the reactants were perfectly dissolved, 14 g of KOH (5 eq.) were added portion wise, then the reaction was heated up to 90 °C for 2 h. When foam has formed the mixture was heated up again, up to 145 °C for 2h. When the reaction was complete, the mixture was poured onto ice cold water and acidified with 1M HCl. The precipitate was filtered and washed several times with brine to obtain a yellowish powder (56% yield). ^{1}H NMR (300MHz, DMSO-d_6): δ 6.41 (s, 1H, CH), 3.77 (s, 6H, O-CH$_3$), 3.57 (s, 3H, O-CH$_3$), 1.98 (s, 6H, CH$_3$)

4.2.5. Synthesis of 2-hydroxy-3,5-dimethyl-4,6-dimethoxyacetophenone

According to a previously described synthesis [61], 10 g of 2,4-dimethyl-1,3,5-trimethoxybenzene were dissolved in 26 mL of acetic anhydride (5.5 eq.). Then 6.4 mL of boron trifluoride ethyl etherate (2 equimolar) were added dropwise to the mixture. When the addition was completed, the mixture was heated up to 90 °C and stirred for 1.5 h, then the reaction was allowed to stand without stirring overnight. Then, 30 mL of water were added and the mixture was stirred again for 10 min. Twenty-five milliliters of ethyl acetate were added, and the mixture was extracted three times. The organic layers were combined and washed several times with brine, then dried under pressure to obtain a dark brown thick oil (74 % yield).

^{1}H NMR (300MHz, DMSO-d_6): δ 12.81 (s, 1H, OH), 3.71 (s, 3H, O-CH$_3$), 3.69 (s, 3H, O-CH$_3$), 2.65 (s, 3H, COCH$_3$), 2.09 (s, 3H, CH$_3$), 2.03 (s, 3H, CH$_3$)

4.2.6. Synthesis of 2-hydroxy-3,5-dimethyl-4,6-dimethoxychalcone

To 10 mL of ethanol were added 0.224 g of 2-hydroxy-3,5-dimethyl-4,6-dimethoxyacetophenone, 0.106 g of benzaldehyde (1 eq.) and 0.168 g of lithium hydroxide (5 eq.). The mixture was then stirred at room temperature for 16 h. Then, ethanol was evaporated under pressure and the residual oil was washed with water and 1M HCl. The precipitate is filtered then dissolved in ethyl acetate. The mixture was extracted several times with brine and ethyl acetate evaporated to obtain a bright orange oil (89% yield). ^{1}H NMR (300 MHz, CDCl$_3$): δ 7.42-7.51 (m, 6H), 5.42 (d, 3Hz, 1H), 3.83 (s, 3H, O-CH$_3$), 3.75 (s, 3H, O-CH$_3$), 2.17 (s, 6H, 2xCH$_3$). ^{13}C NMR (75 MHz, CDCl$_3$): δ 190.2, 163.4, 159.,6, 139.1, 128.7, 125.7, 118.6, 115.6, 111.7, 61.1, 60.0, 8.5, 9.0

4.2.7. Synthesis of 3,5-dimethyl-2,4,6-dimethoxychalcone (TriMetChalc)

Two hundred milligrams of 2-hydroxy-3,5-dimethyl-4,6-dimethoxychalcone and 265 mg of potassium carbonate (3 eq.) were dissolved in 10 mL of acetone. A volume of 0.121 mL of dimethyl sulfate (2 eq.) were added dropwise, and the mixture was stirred and refluxed for 12h. When the reaction was complete, the precipitate was filtered, and the solvent evaporated. The residual oil was dissolved in dichloromethane and extracted several times with brine. The organic layer was evaporated to obtain a bright yellow oil. (76% yield). ^{1}H NMR (300 MHz; CDCl$_3$): δ 7.50 (m, 2H), 7.29 (m, 4H), 6.95 (d, J=15 Hz), 3.65 (s, 3H, O-CH$_3$), 3.59 (s, 6H, 2xO-CH$_3$), 2.13 (s, 6H, 2xCH$_3$). ^{13}C NMR (75 MHz; CDCl$_3$): δ 193.3, 162.0, 159.1, 158.9, 142.8, 135.4, 130.1, 128.9, 128.4, 126.7, 109.1, 108.8, 106.5, 62.3, 8.2, 7.5.

4.3. *Per os administration of TriMetChalc*

Once a day (i.e., 10h AM), mice were administered 6.25 to 25 mg/kg body weight (BW) TriMetChalc dissolved in vegetal oil via gavage using a 22 gauge intubation needle (Popper and Sons). Prior to TriMetChalc treatment, mice received the same volume of distilled water using the similar oral administration procedure for a habituation period of seven consecutive days.

4.4. *Food Intake Measurements and Pica Behavior (Kaolin Intake)*

Food consumption: Immediately after treatment, a new supply of pre-weighed food was given. Food intake was calculated as the difference between the pre-weighed food and the remaining chow measured with a precision balance (0.01 g; Denver Instrument from Bioblock).

Measurement of pica behavior (kaolin intake): Pica behavior was assayed as previously described [20]. Briefly, kaolin pellets were prepared from pharmacological grade kaolin and gum Arabic (Sigma Chemical Co) mixed at a 99:1 ratio in distilled water. The kaolin paste was rolled and cut into pieces similar in shape to mice chow pellets. The pellets were dried in an oven at 37 °C for 72h and then placed in individual cages. Mice were allowed access to regular food and kaolin pellets for a 5 days adaptation period before the beginning of the study. On the day of the experiment the last 24h, the kaolin consumption was recorded. Mice were then *per os* administered TriMetChal (65 mg/kg BW) or vehicle as described above and kaolin intake was measured 24h later by subtracting pre-weighed and remaining kaolin pellets with a precision balance (Denver Instrument from Bioblock).

4.5. *Tissue histology and Oil Red O staining*

Oil Red O (ORO) staining of hepatic sections was performed as previously described [62]. Briefly, 10 μm thick sections were prepared from fixed liver samples with a cryostat (Leica CM3050, France). ORO stock solution 0.625 % was first prepared in isopropanol. Sections were then incubated 6 min in ORO working solution (1.5 parts of ORO stock solution to one part of distilled water) and then washed three times in distilled water. For microscopic observations, sections were mounted in Mowiol solution. Four microphotographs (x 20) per animal were acquired using a Nikon Eclipse E600

light microscope coupled to a DXM 1200 Camera and ACT-1 software. The number of lipid droplets per surface unity (mm^2), total droplet surface per surface unity (mm^2) and lipid droplet size were counted for each condition using the NIH Image J software.

4.6. Immunohistochemistry Procedures

Per os treated-animals used for immunostaining procedure were sacrificed 3h after treatment without free access to food. Mice were anaesthetized using intraperitoneal injection (ip) of ketamine (120 mg/kg BW, Imalgène 1000, Boehringer Ingelheim) and xylazine (16 mg/kg BW, Rompun 2%, Bayer Santé). Intracardiac perfusion was achieved in 4% paraformaldehyde (PFA). Brains were post-fixed for 1h in 4% PFA at room temperature, rinsed in PBS and then cryoprotected for 24-48 h in 30% sucrose at 4°C. After freezing of the brains in isopentane (-40°C), coronal sections (40 μm thick) were cut on a cryostat (Leica CM3050, France) and collected serially in PBS (0.1 M; pH 7.4). Brains were cut from caudal brainstem (Bregma -8.24 mm) to forebrain (Bregma + 0.75 mm).

c-Fos immunohistochemistry was performed on free-floating sections using an anti-c-Fos rabbit antiserum synthesized against the N-terminus of human protein (1:3000, Millipore) as previously described [22]. Briefly, the free-floating sections were incubated 10 min in a solution containing 0.3% H$_2$O$_2$ in PBS 0.1 M for quenching of endogenous peroxidase activity. The sections were first incubated 1h in PBS containing 3% normal goat serum (NGS) and 0.3% Triton X-100, then for overnight at room temperature in PBS containing 3% NGS, 0.3% Triton X-100 and anti-c-Fos antibody. A biotinylated goat anti-rabbit IgG (1:400, Vector Labs) was used as secondary antibody. After incubation with the avidin-biotin complex (1:200, Vector Labs), horseradish peroxidase activity was visualized using a nickel-enhanced diaminobenzidine (DAB) as the chromogen. The reaction was closely monitored and terminated when optimal intensity was reached (3-5 min) by washing the sections in distilled water. Non-specific labeling was assessed on alternate slices that were processed identically to those above but in which the primary antibody was omitted. Finally, all sections were mounted on gelatin-coated slides, air dried, and coverslipped with mounting medium.

4.7. Microscopy, Image Analysis and Cell Count

c-Fos immunostaining was further analyzed by counting positive nuclei on four sections. c-Fos positive nuclei counting was performed on photomicrographs acquired using a 10x objective equipped with a DXM 1200 Camera (Nikon) coupled to ACT-1 software. The microscope was set to a specific illumination level, as was the camera exposure time. c-Fos positive nuclei were then counted on these pictures by computer-assisted morphometry using the NIH image J software. Images were normalized by subtracting the background determined for each nucleus studied. The c-Fos stained elements were identified by setting a threshold value (140 grey levels above the background on a 0-255 intensity scale). Counts were manually corrected for overlapping cell nuclei that were counted by the software as unique. Software-generated counts of c-Fos stained profiles were also manually corrected by excluding positive objects whose area did not exceed 10 pixels (image resolution 150 pixels/inch) corresponding to objects with an area equal or less than to 3 square μm.

4.8. Extraction and Analysis of Neutral Lipids and Phospholipids

We performed quantitative analysis of neutral lipids (Free Cholesterol, Cholesterol ester C16, C18 and C20:4, Triacylglycerols C49, C51, C53, C55, C57, C59) and of the following classes of phospholipids (PL), ceramides (Cer18:1), phosphatidylethanolamines (PE), phosphatidylcholines (PC), sphingomyelins (SM d18:1), phosphatidylserines (PS), phosphatidylinositols (PI) on liver samples. Internal calibrations were achieved with Stigmasterol, Cholesterol ester C17, TAG 19 for neutral lipids and Cerd18:1/12:0 20 ng, PE 12:0/12:0 180 ng, PC 13:0/13:0 20 ng, SM d18:1/12:0 20 ng, PI 16:0/17:0 30 ng, PS 12:0/12:0 1600 ng for Phospholipids and ceramides. This method allows a relative quantification of the molecules.

For extraction, each frozen liver sample was crushed with a FastPrep ®-24 Instrument (MP Biomedical) in 1mL of Water/EGTA 5mM: Metanol (1:2, v/v). After 2 crush cycles (10 m/s, 2X30 s), lipids were extracted according to Bligh and Dyer in dichloromethane/water/methanol 2% acetic acid (2.5:2:2.5, v/v/v) [63], in the presence 100 μL internal standards of neutral Lipids and 40 μL internal standards of phospholipids. Samples were centrifuged at 2500 revolutions per minute (RPM/min) for 6 min, evaporated to dryness and then dissolved in 20 μL of ethyl acetate of neutral lipids or 50 μL methanol of phospholipids.

For neutral lipids, 1 μL of the lipid extract was analyzed by gas chromatography flam ionization detector on a GC TRACE 1300 Thermo Electron system using an Zebron ZB-5MS Phenomenex columns (5% polysilarylene, 95% polydimethylsiloxane, 5 m X 0.25 mm i.d, 0.25 μm film thickness [64]. Oven temperature was programmed from 190°C to 350 °C at a rate of 5°C/min and the carrier gas was hydrogen (5 mL/min). The injector and the detector were at 315 °C and 345 °C respectively.

For phospholipids, lipid extracts were analyzed by liquid chromatography mass spectrometry using an Agilent 1290 UPLC system coupled to a G6460 triple quadripole mass spectrometer (Agilent Technologies) and using MassHunter software for data acquisition and analysis. A Kinetex HILIC column (Phenomenex, 50 x 4.6 mm, 2.6 μm) was used for liquid chromatography separations. The column temperature was controlled at 40°C. The mobile phase A was acetonitrile and phase B was 10 mM ammonium formate in water at pH 3.2. For Cer, PE, PC, SM: the gradient was as follows: from 10% to 30% B in 10 min; 10-12 min, 100% B; and then back to 10% B at 13 min for 2 min prior to the next injection. The flow rate of mobile phase was 0.3 mL/min and the injection volume was 2 μL. For PI, PS: the gradient was as follows: from 5% to 50% B in 10 min and then back to 5% B at 10.2 min for 9 min prior to the next injection. The flow rate of mobile phase was 0.8 mL/min and the injection volume was 5 μL. Electrospray ionization was performed in positive mode for Cer, PE, PC and SM analysis and in negative mode for PI and PS analysis. Needle voltage was set respectively at 4 kV and -3.5 kV. Analyses were performed in Selected Reaction Monitoring detection mode (SRM) using nitrogen as collision gas. Ion optics and collision energy were optimized for each lipid class. Finally, peak detection, integration and quantitative analysis were done using MassHunter Quantitative analysis software (Agilent Technologies).

4.9. Extraction and Analysis of Fatty Acids

Quantitative analysis of total conventional fatty acids (FAs, c10:0, c12:0, c14:0, c15:0, c16:0, c17:0, c18:0, c20:0, c22:0, c23:0, c24:0, c14:1w5, c15:1, c16:1w7, c18:1w9, c18:1w7, c20:1w9, c22:1w9, c24:1w9, c18:2w6, c18:3w6, c18:3w3, c20:2w6 , c20:3w3, c20:3w6, c20:4w6, c20:5w3, c22:2w6, c22:6w3, c22:4w6) was achieved using TAG17 or TAG19 or TAG15 as internal standard. This method allows a relative quantification of esterified and free fatty acids. Lipids were extracted according to Bligh and Dyer ([63] in dichloromethane/methanol/water (2.5:2.5:2, v/v/v), in the presence of the internal standards glyceryl trinonadecanoate (4 μg). The lipid extract was hydrolyzed in KOH (0.5 M in methanol) at 55°C for 30 min, and transmethylated in boron trifluoride methanol solution 14% (SIGMA, 1 mL) and heptane (1 mL) at 80°C for 1h. After addition of water (1 mL) to the crude, FAs were extracted with heptane (3 mL), evaporated to dryness and dissolved in ethyl acetate (20 μL). FAs were analyzed by gas chromatography equipped with a FID on a Clarus 600 Perkin Elmer system using a Famewax RESTEK fused silica capillary columns (30 m x 0.32 mm i.d, 0.25 μm film thickness) [65]. Oven temperature was programmed from 100°C to 250°C at a rate of 6°C/min and the carrier gas was hydrogen (1.5mL/min). The injector and the detector were at 220°C and 230°C respectively.

4.10. Statistical Analysis

All results are presented as mean ± SEM. Statistical analyses were performed using Graphpad Prism 6.05. Comparison between two groups was performed using unpaired 2-tailed Student's t test. Pearson correlation analysis was used to quantify relationships between variables of interest. Significant difference was assessed by a one-way ANOVA followed by a *post hoc* Fisher's test for comparison between four or five groups (fig 2, 4, 6F). Two ways ANOVAs followed by Bonferroni's

multiple comparisons were used to assess effects at different time post treatment (fig 6A and C). *P*-values less than 0.05 were considered significant.

5. Conclusions

In summary, the present work provides the first demonstration of a chalcone derivative capable of reducing both food intake and hepatic steatosis in a mouse model of obesity and MAFLD. Given that in obese subjects, insulin-resistant hypertrophic white adipocytes exhibit high elevated lipolysis, which explains the link between obesity and MAFLD, we cannot exclude that the reduction in food intake and overweight induced by TriMetChalc partly explain the amelioration of MAFLD. Although promising, these results need to be supplemented with additional studies which will clarify its mode of action and evaluate its action over longer treatment periods and/or in combination with other chalcones with protective effects on the liver.

References

1. WHO **2016**; World Health Organization. Obesity and Overweight. Available online: https://www.who.int/news-room/fact-sheets/de- 854tail/obesity-and-overweight.
2. Mitra, S.; De, A.; Chowdhury, A. Epidemiology of non-alcoholic and alcoholic fatty liver diseases. *Transl. Gastroenterol. Hepatol*. **2020**, *5*, 16. https://doi.org/10.21037/tgh.2019.09.08.
3. Heeren, J.; Scheja, L. Metabolic-associated fatty liver disease and lipoprotein metabolism. *Mol. Metab.* **2021,** *50*,101238. https://doi.org/10.1016/j.molmet.2021.101238.
4. Eslam, M.; Newsome, P.N.; Sarin, S.K.; Anstee, Q.M.; Targher, G.; Romero-Gomez, M.; Zelber-Sagi, S.; Wong, V.W.S.; Dufour, J.F.; Schattenberg, J.M.; et al. A new definition for metabolic dysfunction-associated fatty liver disease: An international expert consensus statement. *J. Hepatol.* **2020**, *73*, 202–209. https://doi.org/10.1016/j.jhep.2020.03.039.
5. Gofton, C.; Upendran, Y.; Zheng, M.H.; George, J. MAFLD: How is it different from NAFLD? *Clin. Mol. Hepatol.* **2023**, *29*, S17–S31. https://doi.org/10.3350/cmh.2022.0367.
6. Younossi, Z.M.; Koenig, A.B.; Abdelatif, D.; Fazel, Y.; Henry, L.; Wymer, M. Global epidemiology of nonalcoholic fatty liver disease: Meta-analytic assessment of prevalence, incidence, and outcomes. *Hepatology* **2016**, *64*, 73–84. https://doi.org/10.1002/hep.28431.
7. Liu, J.; Ayada, I.; Zhang, X.; Wang, L.; Li, Y.; Wen, T.; Ma, Z.; Bruno, M.J.; de Knegt, R.J.; Cao, W. et al. Estimating Global Prevalence of Metabolic Dysfunction-Associated Fatty Liver Disease in Overweight or Obese Adults. *Clin. Gastroenterol. Hepatol.* **2022**, *20*, e573–e582. https://doi.org/10.1016/j.cgh.2021.02.030.
8. Fabbrini, E.; Sullivan, S.; Klein, S. Obesity and nonalcoholic fatty liver disease: Biochemical, metabolic, and clinical implications. *Hepatology* **2010**, *51*, 679–689. https://doi.org/10.1002/hep.23280.
9. Karimi-Sales, E.; Mohaddes, G.; Alipour, M.R. Chalcones as putative hepatoprotective agents: Preclinical evidence and molecular mechanisms. *Pharmacol. Res.* **2018**, *129*, 177–187. https://doi.org/10.1016/j.phrs.2017.11.022.

10. Mai, T.T. ; Chuyen, N.V. Anti-hyperglycemic activity of an aqueous extract from flower buds of Cleistocalyx operculatus (Roxb.) Merr and Perry. *Biosci. Biotechnol. Biochem.* **2007**, *71*, 69–76. https://doi.org/10.1271/bbb.60373.

11. Hu, Y.C.; Zhang, Z.; Shi, W.G.; Mi, T.Y.; Zhou, L.X.; Huang, N.; Hoptroff, M.; Lu, Y.H. 2′,4′-dihydroxy-6′-methoxy-3′,5′-dimethylchalcone promoted glucose uptake and imposed a paradoxical effect on adipocyte differentiation in 3T3-L1 cells. *J. Agric. Food. Chem.* **2014**, *62*, 1898–1904. https://doi.org/10.1021/jf405368q.

12. Choi, J.W.; Kim, M.; Song, H.; Lee, C.S.; Oh, W.K.; Mook-Jung, I.; Chung, S.S.; Park, K.S. DMC (2′,4′-dihydroxy-6′-methoxy-3′,5′-dimethylchalcone) improves glucose tolerance as a potent AMPK activator. *Metabolism.* **2016**, *65*, 533–542.. https://doi.org/10.1016/j.metabol.2015.12.010.

13. Benny, F.; Kumar, S.; Binu, A.; Parambi, D.G.T.; Alsahli, T.G. Al-Sehemi, A.G.; Chandran, N.; Manisha, D.S.; Sreekumar, S.; Bhatt, A. et al. Targeting GABA receptors with chalcone derivative compounds, what is the evidence? *Expert Opin. Ther. Targets* **2023**, *27*, 1257–1269. https://doi.org/10.1080/14728222.2023.2293752. 38112471.

14. Dadi, V.; Malla, R.R.; Siragam, S. Natural and Synthetic Chalcones: Potential Impact on Breast Cancer. *Crit. Rev. Oncog.* **2023**, *28*, 27–40. https://doi.org/10.1615/CritRevOncog.2023049659.

15. Nematollahi, M.H.; Mehrabani, M.; Hozhabri, Y.; Mirtajaddini, M.; Iravani, S. Antiviraland antimicrobial applications of chalcones and their derivatives: From nature to greener synthesis. *Heliyon* **2023**, *9*, e20428. https://doi.org/10.1016/j.heliyon.2023.e20428.

16. Trak-Smayra, V.; Paradis, V.; Massart, J.; Nasser, S.; Jebara, V.; Fromenty, B. Pathology of the liver in obese and diabetic ob/ob and db/db mice fed a standard or high-calorie diet. *Int. J. Exp. Pathol.* **2011**, *92*, 413–421.. https://doi.org/10.1111/j.1365-2613.2011.00793.x.

17. Parlati, L.; Régnier, M.; Guillou, H.; Postic, C. New targets for NAFLD. *JHEP Rep.* **2021**, *3*, 100346. https://doi.org/10.1016/j.jhepr.2021.100346.

18. Roth, C.L.; McCormack, S.E. Acquired hypothalamic obesity: A clinical overview and update. *Diabetes Obes. Metab.* **2024**, *26*, 34–45. https://doi.org/10.1111/dom.15530.

19. Porter, M.H.; Arnold, M.; Langhans, W. Lipopolysaccharide-induced anorexia following hepatic portal vein and vena cava administration. *Physiol. Behav.* **1998**, *64*, 581–584. https://doi.org/10.1016/s0031-9384(98)00082-1.

20. Girardet, C.; Bonnet, M.S.; Jdir, R.; Sadoud, M.; Thirion, S.; Tardivel, C.; Roux, J.; Lebrun, B.; Wanaverbecq, N.; Mounien, L. et al. The food-contaminant deoxynivalenol modifies eating by targeting anorexigenic neurocircuitry. *PLoS ONE.* **2011**, *6*, e26134. https://doi.org/10.1371/journal.pone.0026134.

21. Brüning, J.C.; Fenselau, H. Integrative neurocircuits that control metabolism and food intake. *Science* **2023**, *381*, eabl7398. https://doi.org/10.1126/science.abl7398.

22. Guillebaud, F.; Duquenne, M.; Djelloul, M.; Pierre, C.; Poirot, K.; Roussel, G.; Riad, S.; Lanfray, D.; Morin, F.; Jean, A. et al. Glial Endozepines Reverse High-Fat Diet-Induced Obesity by Enhancing Hypothalamic Response to Peripheral Leptin. *Mol. Neurobiol.* **2020**, *57*, 3307–3333. https://doi.org/10.1007/s12035-020-01944-z.

23. Gaige, S.; Barbouche, R.; Barbot, M.; Boularand, S.; Dallaporta, M.; Abysique, A.; Troadec, J.D. Constitutively active microglial populations limit anorexia induced by the food contaminant deoxynivalenol. *J. Neuroinflammation* **2022**, *19*, 280. https://doi.org/10.1186/s12974-022-02631-7.

24. Xue, B.; Kahn, B.B. AMPK integrates nutrient and hormonal signals to regulate food intake and energy balance through effects in the hypothalamus and peripheral tissues. *J. Physiol.* **2006**, *574*, 73–83. https://doi.org/10.1113/jphysiol.2006.113217.

25. Minokoshi, Y.; Alquier, T.; Furukawa, N.; Kim, Y.B.; Lee, A.; Xue, B. Mu, J.; Foufelle, F.; Ferré, P.; Birnbaum, M.J. et al. AMP-kinase regulates food intake by responding to hormonal and nutrient signals in the hypothalamus. *Nature* **2004**, *428*, 569–574. https://doi.org/10.1038/nature02440.

26. López, M. Hypothalamic AMPK and energy balance. *Eur. J. Clin. Invest.* **2018**, *48*, e12996. https://doi.org/10.1111/eci.12996.

27. Lee, J.S.; Chun, H.C.; Choi, J.Y; Park, K.S.; Chung, S.S.; Park, K. Synthesis of 2′,4′,6′-trimethoxy-3′,5′-dimethylchalcone derivatives and their anti-diabetic and anti-atherosclerosis effect. *Journal of Industrial and Engineering Chemistry* **2023**, *128*, 268–274. doi.org/10.1016/j.jiec.2023.07.058.

28. Hsieh, C.T.; Chang, F.R.; Tsai, Y.H.; Wu, Y.C.; Hsieh, T.J. 2-Bromo-4′-methoxychalcone and 2-Iodo-4′-methoxychalcone Prevent Progression of Hyperglycemia and Obesity via 5′-Adenosine-Monophosphate-Activated Protein Kinase in Diet-Induced Obese Mice. *Int. J. Mol. Sci.* **2018**, *19*, 2763. https://doi.org/10.3390/ijms19092763.

29. Ludwig, J.; Viggiano, T.R.; McGill, D.B.; Oh, B.J. Nonalcoholic steatohepatitis: Mayo Clinic experiences with a hitherto unnamed disease. *Mayo Clin. Proc.* **1980**, *55*, 434–438. PMID: 7382552.

30. Samy, A.M.; Kandeil, M.A.; Sabry, D.; Abdel-Ghany, A.A.; Mahmoud, M.O. From NAFLD to NASH: Understanding the spectrum of non-alcoholic liver diseases and their consequences. *Heliyon* **2024**, *10*, e30387. https://doi.org/10.1016/j.heliyon.2024.e30387.

31. Yu, W.G.; Qian, J.; Lu, Y.H. Hepatoprotective effects of 2',4'-dihydroxy-6'-methoxy-3',5'-dimethylchalcone on CCl4-induced acute liver injury in mice. *J. Agric. Food Chem*. **2011**, *59*, 12821–12829. https://doi.org/10.1021/jf2042032.

32. Hliwa, A.; Ramos-Molina, B.; Laski, D.; Mika, A.; Sledzinski, T. The role of fatty acids in non-alcoholic fatty liver disease progression: An Update. *Int. J. Mol. Sci.* **2021**, *22*, 6900. https://doi.org/10.3390/ijms22136900.

33. Malhi, H.; Bronk, S.F.; Werneburg, N.W.; Gores, G.J. Free fatty acids induce JNK-dependent hepatocyte lipoapoptosis. *J. Biol. Chem.* **2006**, *281*, 12093–12101. https://doi.org/10.1074/jbc.M510660200.

34. Malhi, H.; Gores, G.J. Molecular mechanisms of lipotoxicity in nonalcoholic fatty liver disease. *Semin. Liver Dis.* **2008**, *28*, 360–369.. https://doi.org/10.1055/s-0028-1091980.

35. Miura, K.; Yang, L.; van Rooijen, N.; Brenner, D.A.; Ohnishi, H.; Seki, E. Toll-likereceptor 2 and palmitic acid cooperatively contribute to the development of nonalcoholic steatohepatitis through inflammasome activation in mice. *Hepatology* **2013**, *57*, 577–589.. https://doi.org/10.1002/hep.26081.

36. Lottenberg, A.M.; Afonso Mda, S.; Lavrador, M.S.; Machado, R.M.; Nakandakare, E.R. The role of dietary fatty acids in the pathology of metabolic syndrome. *J. Nutr. Biochem.* **2012**, *23*, 1027–1040. doi : 10.1016/j.jnutbio.2012.03.004.

37. Wang, X.; Cao, Y.; Fu, Y.; Guo, G.; Zhang, X. Liver fatty acid composition in mice with or without nonalcoholic fatty liver disease. *Lipids Health Dis.* **2011**, *10*, 234. https://doi.org/10.1186/1476-511X-10-234.

38. Puri, P.; Baillie, R.A.; Wiest, M.M.; Mirshahi, F.; Choudhury, J.; Cheung, O.; Sargeant, C.; Contos, M.J.; Sanyal, A.J. A lipidomic analysis of nonalcoholic fatty liver disease. *Hepatology* **2007**, *46*, 1081–1090. https://doi.org/10.1002/hep.21763.

39. Spooner, M.H.; Jump, D.B. Omega-3 fatty acids and nonalcoholic fatty liver disease in adults and children: Where do we stand? *Curr. Opin. Clin. Nutr. Metab. Care* **2019**, *22*, 103–110.. https://doi.org/10.1097/MCO.0000000000000539.

40. Musso, G.; Cassader, M.; Paschetta, E.; Gambino, R. Bioactive lipid species and metabolic pathways in progression and resolution of nonalcoholic steatohepatitis. *Gastroenterology* **2018**, *155*, 282–302.e8. https://doi.org/10.1053/j.gastro.2018.06.031.

41. Yan, D.; Dou, Q.L.; Wang, Z.; Wei, Y. Y.. Establishment of a hepatocyte steatosis model using Chang liver cells. *Genet. Mol. Res.* **2015**, *14*,15224–15232. https://doi.org/10.4238/2015.November.25.10.

42. Hu, J.; Hong, W.; Yao, K.N.; Zhu, X.H.; Chen, Z.Y.; Ye, L. Ursodeoxycholic acid ameliorates hepatic lipid metabolism in LO2 cells by regulating the AKT/mTOR/SREBP-1 signaling pathway. *World J. Gastroenterol.* **2019** *25*, 1492–1501. https://doi.org/10.3748/wjg.v25.i12.1492.

43. Akazawa, Y.; Cazanave, S.; Mott, J.L.; Elmi, N.; Bronk, S.F.; Kohno, S.; Charlton, M.R.; Gores, G.J. Palmitoleate attenuates palmitate-induced Bim and PUMA upregulation and hepatocyte lipoapoptosis. *J. Hepatol.* **2010**, *52*, 586–593. https://doi.org/10.1016/j.jhep.2010.01.003.

44. Listenberger, L.L.; Han, X.; Lewis, S.E.; Cases, S.; Farese Jr, R.V.; Ory, D.S.; Schaffer, J.E. Triglyceride accumulation protects against fatty acid-induced lipotoxicity. *Proc. Natl. Acad. Sci. USA* **2003**,*100*, 3077–3082. https://doi.org/10.1073/pnas.0630588100.

45. .

46. Kurikawa, N.; Takagi, T.; Wakimoto, S.; Uto, Y.; Terashima, H.; Kono, K.; Ogata, T.; Ohsumi, J. A novel inhibitor of stearoyl-CoA desaturase-1 attenuates hepatic lipid accumulation, liver injury and inflammation in model of nonalcoholic steatohepatitis. *Biol. Pharm. Bull.* **2013**, *36*, 259–267. https://doi.org/10.1248/bpb.b12-00702.

47. Uto, Y. Recent progress in the discovery and development of stearoyl CoA desaturase inhibitors. *Chem. Phys. Lipids* **2016**, *197*, 3–12. https://doi.org/10.1016/j.chemphyslip.2015.08.018.

48. Nobili, V.; Alisi, A.; Musso, G.; Scorletti, E.; Calder, P.C.; Byrne, C.D. Omega-3 fatty acids: Mechanisms of benefit and therapeutic effects in pediatric and adult NAFLD. *Crit. Rev. Clin. Lab. Sci.* **2016**, *53*, 106–120. https://doi.org/10.3109/10408363.2015.1092106.

49. Chiappini, F.; Coilly, A.; Kadar, H.; Gual, P.; Tran, A.; Desterke, C.; Samuel, D.; Duclos-Vallée, J.C.; Touboul, D.; Bertrand-Michel, J.; et al. Metabolism dysregulation induces a specific lipid signature of nonalcoholic steatohepatitis in patients. *Sci. Rep.* **2017**, *7*, 1–17. https://doi.org/10.1038/srep46658.

50. Schaefer, E.J. Lipoproteins, nutrition, and heart disease. *Am. J. Clin. Nutr.* **2002**, *75*, 191–212. https://doi.org/10.1093/ajcn/75.2.191.

51. Yu, L.; Yuan, M.; Wang, L. The effect of Omega-3 unsaturated fatty acids on non-alcoholic fatty liver disease: A systematic review and meta-analysis of RCTs. *Pak. J. Med. Sci.* **2017**, *33*, 1022–1028.. https://doi.org/10.12669/pjms.334.12315.

52. Figueiredo, P.S.; Carla Inada, A.; Marcelino, G.; Maiara Lopes Cardozo, C.; de Cássia Freitas, K.; de Cássia Avellaneda Guimarães, R.; Pereira de Castro, A.; Aragão do Nascimento, V.; Aiko Hiane, P. Fatty acids consumption: The role metabolic aspects involved in obesity and its associated disorders. *Nutrients* **2017**, *22*, 1158. https://doi.org/10.3390/nu9101158.

53. Diraison, F.; Moulin, P.; Beylot, M. Contribution of hepatic de novo lipogenesis and reesterification of plasma non esterified fatty acids to plasma triglyceride synthesis during non-alcoholic fatty liver disease. *Diabetes Metab.* **2003**, *29*, 478e485. https://doi.org/10.1016/s1262-3636(07)70061-7.

54. Hudgins, L.C.; Hellerstein, M.; Seidman, C.; Neese, R.; Diakun, J.; Hirsch, J. Human fatty acid synthesis is stimulated by a eucaloric low fat, high carbohydrate diet. *J. Clin. Invest.* **1996**, *97*, 2081–2091.. https://doi.org/10.1172/JCI118645.

55. Hayakawa, J.; Wang, M.; Wang, C.; Han, R.H.; Jiang, Z.Y.; Han, X. Lipidomic analysis reveals significant lipogenesis and accumulation of lipotoxic components in ob/ob mouse organs. *Prostaglandins Leukot. Essent. Fatty Acids* **2018**, *136*, 161–169. https://doi.org/10.1016/j.plefa.2017.01.002.

56. Fu, S.; Yang, L.; Li, P.; Hofmann, O.; Dicker, L.; Hide, W.; Lin, X.; Watkins, S.M.; Ivanov, A.R.; Hotamisligil, G.S. Aberrant lipid metabolism disrupts calcium homeostasis causing liver endoplasmic reticulum stress in obesity. *Nature* **2011**, *473*, 528–531. https://doi.org/10.1038/nature09968.

57. Ling, J.; Chaba, T.; Zhu, L.F.; Jacobs, R.L.; Vance, D.E. Hepatic ratio of phosphatidylcholine to phosphatidylethanolamine predicts survival after partial hepatectomy in mice. *Hepatology* **2012**, *55*, 1094–1102. https://doi.org/10.1002/hep.24782.

58. van der Veen, J.N.; Kennelly, J.P.; Wan, S.; Vance, J.E.; Vance, D.E.; Jacobs, R.L. The critical role of phosphatidylcholine and phosphatidylethanolamine metabolism in health and disease. *Biochim. Biophys. Acta BBA Biomembr.* **2017**, *1859*, 1558–1572. https://doi.org/10.1016/j.bbamem.2017.04.006.

59. Perfield 2nd, J.W.; Ortinau, L.C.; Pickering, R.T.; Ruebel, M.L.; Meers, G.M.; Rector, R.S. Altered hepatic lipid metabolism contributes to nonalcoholic fatty liver disease in leptin-deficient Ob/Ob mice, *J. Obes.* **2013**, 296537. https://doi.org/10.1155/2013/296537.

60. Babu, A.V.; Rambabu, A.; Giriprasad, P.V.; Rao, R.S.C.; Babu, B.H. Synthesis of (±)-Pisonivanone and Other Analogs as Potent Antituberculosis Agents. *J. Chem*. **2012**, *2013*, 961201. doi.org/10.1155/2013/961201.

61. Anandam, R.; Jadav, S.S.; Ala, V.B.; Ahsan, M.J.; Bollikolla, H.B. Synthesis of new C-dimethylated chalcones as potent antitubercular agents. *Med. Chem. Res*. **2018**, *27*, 1690–1704. doi.10.1007/s00044-018-2183-z.

62. Jung, J.W.; Damodar, K.; Kim, J.K.; Jun, J.G. First synthesis and in vitro biological assessment of isosideroxylin, 6,8-dimethylgenistein and their analogues as nitric oxide production inhibition agents. *Chin. Chem. Lett*. **2017**, *28*, 1114-1118. doi.org/10.1016/j.cclet.2016.12.041.

63. Barbouche, R.; Gaigé, S.; Airault, C.; Poirot, K.; Dallaporta, M.; Troadec, J.D.; Abysique, A. The food contaminant deoxynivalenol provokes metabolic impairments resulting in non-alcoholic fatty liver (NAFL) in mice. *Sci. Rep*. **2020**, *10*, 12072. https://doi.org/10.1038/s41598-020-68712-w.

64. Bligh, E.G.; Dyer, W.J. A rapid method of total lipid extraction and purification. *Can. J. Biochem. Physiol.* **1959**, *37*, 911–917.. https://doi.org/10.1139/o59-099.

65. Barrans, A.; Collet, X.; Barbaras, R.; Jaspard, B.; Manent, J.; Vieu, C.; Chap, H.; Perret, B. Hepatic lipase induces the formation of pre-beta 1 high density lipoprotein (HDL) from triacylglycerol-rich HDL2. A study comparing liver perfusion to in vitro incubation with lipases. *J. Biol. Chem.* **1994**, *269*, 11572–11577. PMID: 8157689.

66. Lillington, J.M.; Trafford, D.J.; Makin, H.L. A rapid and simple method for the esterification of fatty acids and steroid carboxylic acids prior to gas-liquid chromatography. *Clin. Chim. Acta*. **1981**, *111*, 91–98.. https://doi.org/10.1016/0009-8981(81)90425-3.